Exhumation of the Western Alpine collisional wedge: New thermochronological data

J.B. Girault, N. Bellahsen, M. Bernet, R. Pik, N. Loget, Eric Lasseur, C.L. Rosenberg, M. Balvay, M. Sonnet

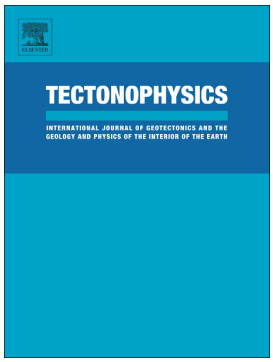

Exhumation of the Western Alpine collisional wedge: New thermochronological data

J.B. Girault, N. Bellahsen, M. Bernet, R. Pik, N. Loget, E. Lasseur, C.L. Rosenberg, M. Balvay, M. Sonnet

PII: S0040-1951(21)00437-6

DOI: https://doi.org/10.1016/j.tecto.2021.229155

Reference: TECTO 229155

To appear in: *Tectonophysics*

Received date: 16 March 2021

Revised date: 13 October 2021

Accepted date: 14 November 2021

Please cite this article as: J.B. Girault, N. Bellahsen, M. Bernet, et al., Exhumation of the Western Alpine collisional wedge: New thermochronological data, *Tectonophysics* (2021), https://doi.org/10.1016/j.tecto.2021.229155

Exhumation of the Western Alpine collisional wedge: new thermochronological data

J.B. Girault[1], N. Bellahsen[1], M. Bernet[2], R. Pik[3], N. Loget[1], E. Lasseur[4], C. L. Rosenberg[1], M. Balvay[2], M. Sonnet[1]

[1] Sorbonne Université, CNRS-INSU, Institut des Sciences de la Terre de Paris, ISTeP UMR 7193, F-75005 Paris, France
[2] Institut des Sciences de la Terre, Université Grenoble Alpes, CNRS, 1381 Rue de la piscine, 38041 Grenoble cedex, France
[3] CRPG, UMR 7358 CNRS-Université de Lorraine, BP20, 15 rue Notre-Dame des Pauvres, 54500 Vandoeuvre-lès-Nancy, France
[4] BRGM - French Geological Survey, 3 Avenue Claude Guillemin, 45100, Orléans, France

Corresponding author: jean-baptiste.girault@sorbonne-universite.fr

Keywords: External Alps, Thermochronology, fission-track analysis, U-Th-Sm/He, Collision, Foreland basin

Abstract

Collisional shortening in the external Western Alps was first accommodated by internal (distributed) deformation in the External Crystalline Massifs (ECM) and then on frontal crustal ramps (localized deformation). However, the timing of transition between these two periods is still under-constrained, mainly because the available dataset is incomplete in the Western Alps. We here provide new zircon and apatite fission-track (ZFT and AFT) and zircon (U-Th-Sm)/He (ZHe) data that constrain the early stages of cooling hence exhumation of the external Alpine wedge, as well as new Raman Spectroscopy of Carbonaceous Material (RSCM) data from the Belledonne massif. ZFT ages mainly range between 15 and 20 Ma, ZHe ages between 5 and 12 Ma, AFT ages between 2 and 10 Ma. Those data are integrated within HeFTy (inverse and forward) thermal models along with literature data to constrain the late Oligocene-Miocene cooling history and suggest that exhumation of the Belledonne and

the Pelvoux massifs may have started as early as ca. 27 Ma. This early exhumation was rather slow (~ 50 m.Myrs^{-1} ± 2 m.Myrs^{-1}) and may date the transition between the distributed and the localized mode of shortening, i.e., the initiation of the crustal ramps below these massifs. Further north, in the Mont Blanc and Aiguilles Rouges massifs, exhumation was active around 18 Ma, and started possibly earlier, around 20-25 Ma. From this time on (18 Ma), exhumation rates increased in all external massifs (~ 500 ± 40 m.Myrs^{-1}, both North and South). This age most likely corresponds to the end of the transition period between distributed and localised shortening with localisation along the frontal crustal ramps and the rapid associated exhumation, then cooling of the hanging-wall (even considering that cooling may start a few Myrs later than exhumation if isoterms are advected). This timing notably corresponds to a transition between the two molasse mega-sequences in the foreland basin (Lower Marine/Freshwater Molasse and Upper Marine/Freshwater Molasse).

1. Introduction

The collision stage of convergence is characterized by crustal accretion of tectonic units under Barrovian metamorphic conditions and formation of molasse basins related to both the erosion in the wedge and flexural subsidence in peri-orogenic domains. Collisional wedges deform either by distributed deformation and/or by more localized deformation along large thrusts. However, if it is frequently observed that one of these deformation modes largely dominates (e.g., Schmid et al., 1996; Burkhard and Sommaruga, 1998; Bellanger et al., 2015), the amount and timing of the distributed deformation is usually poorly documented mainly because of the lack of markers in the internal orogens and/or the lack of deformation ages on brittle/ductile shear zones developed under greenschist metamorphic conditions (with rather small metamorphic minerals). The foreland basins usually develop as a consequence of crustal thickening, associated flexural subsidence and wedge erosion. However, the effect of mode of

wedge shortening (distributed vs. localized) during the overfilled period (Sinclair et al.) on the basin dynamics is much less constrained.

In the European external Western Alps, two modes of shortening have been characterized (Bellahsen et al., 2014): an early phase of distributed deformation documented in the External Crystalline Massifs (ECM, **Fig. 1**) and attested by the occurrence of distributed reverse shear zones (e.g., Rolland et al. 2003; Leloup et al., 2005; Bellanger et al., 2015) along with vertical structures in a transpressional mode (e.g., Simon-Labric et al., 2009, Sanchez et al., 2011; Herwegh et al., 2020), and a later localized phase associated with the activation of frontal ramps below the ECMs (Deville et al., 1994; Philippe et al., 1998). The transition between these two phases seems to corresponds to the initiation of both the subalpine fold-and-thrust-belt (Burkhard and Sommaruga, 1998; Deville and Chauvière, 2000; Bellahsen et al., 2014) and the onset of the exhumation of the ECM (Boutoux et al., 2016; Herwegh et al., 2020; Berger et al., 2020).

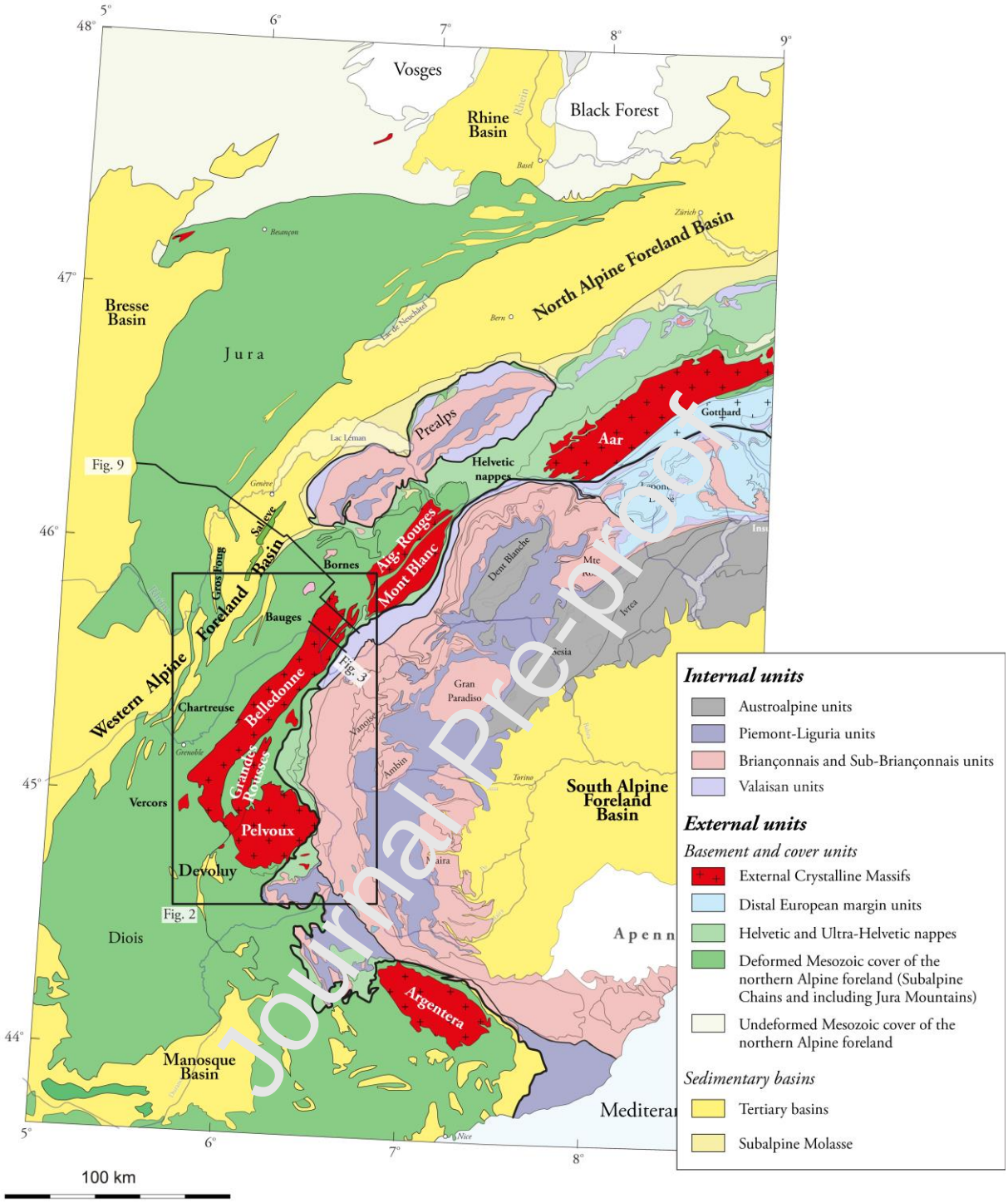

Figure 1: Tectonic map of the western Alpine arc (modified after Bousquet et al., 2012).

Studies on exhumation of the ECMs using low-temperature (LT) thermochronological constraints, showed that exhumation of the northern ECMs (i.e., Mont Blanc and Aiguilles Rouges massifs: Rahn, 1994; Seward and Mancktelow, 1994; Fügenschuh and Schmid, 2003;

Leloup et al., 2005; Glotzbach et al., 2008, 2011; Boutoux et al., 2016; Aar massif: Herwegh et al., 2019; Berger et al., 2019) started around ca. 18-20 Ma although it has been showed that it may have initiated around 20-25 Ma (Schlunegger et al., 1998; von Eynatten et al., 1999; Spiegel et al., 2000), whereas exhumation in the western ECMs, in the Pelvoux and Grandes Rousses massifs, started earlier, at around 27 Ma (e.g., Crouzet et al., 2001; Rolland et al., 2008; van der Beek et al., 2010), although the supporting data are scarce. Thus, the onset of exhumation in the ECM seems to be diachronous from south to north, but this trend remains to be documented due to the lack of LT thermochronological data, especially in the Belledonne ECM.

The overfilled basin dynamics started during early Oligocene times and they are characterized by two transgressive-regressive mega sequences (e.g., Sinclair, 1997; Kempf et al., 1997, 1999). The transition between the two sequences is dated at around 18-20 Ma. Some contributions have discussed the timing between the collisional wedge evolution and the foreland basin (Mosar, 1999; Allen et al., 2001; Willett and Schlunegger, 2010; Schlunegger and Kissling, 2015; Erdös et al., 2019), but none of these was specifically concerned with the impact of exhumation of the ECMs within the orogenic wedge on the foreland basins. More generally, it is noteworthy that the North Alpine Foreland Basin is much developed (both in width and thickness) than the West Alpine Foreland Basin (from Chambery to Mediterranean Sea). No explanation for such first order feature has been reported and it is unclear whether or not the style of shortening and the timing of exhumation may control this along strike difference.

The aim of this contribution is twofold. First, we provide new LT thermochronological data to better constrain exhumation of the ECM in the Western Alps. These data are coupled with new RSCM-based temperature estimates in the sedimentary cover and additional data from the literature to process thermal modeling. These results provide new insights into the

exhumation onset and rates at the scale of the whole external Western Alps. Second, we discuss the links between foreland basin evolution and wedge exhumation, and in particular how the overfilled (molasse) basin evolves during the transition from distributed to localized shortening, along the frontal crustal ramp. A new interpretation of a seismic profile in the molasse basin allows us to define the geometries of sedimentary units and helps discussing the relationships between deformation along the Alpine front and foreland basin evolution.

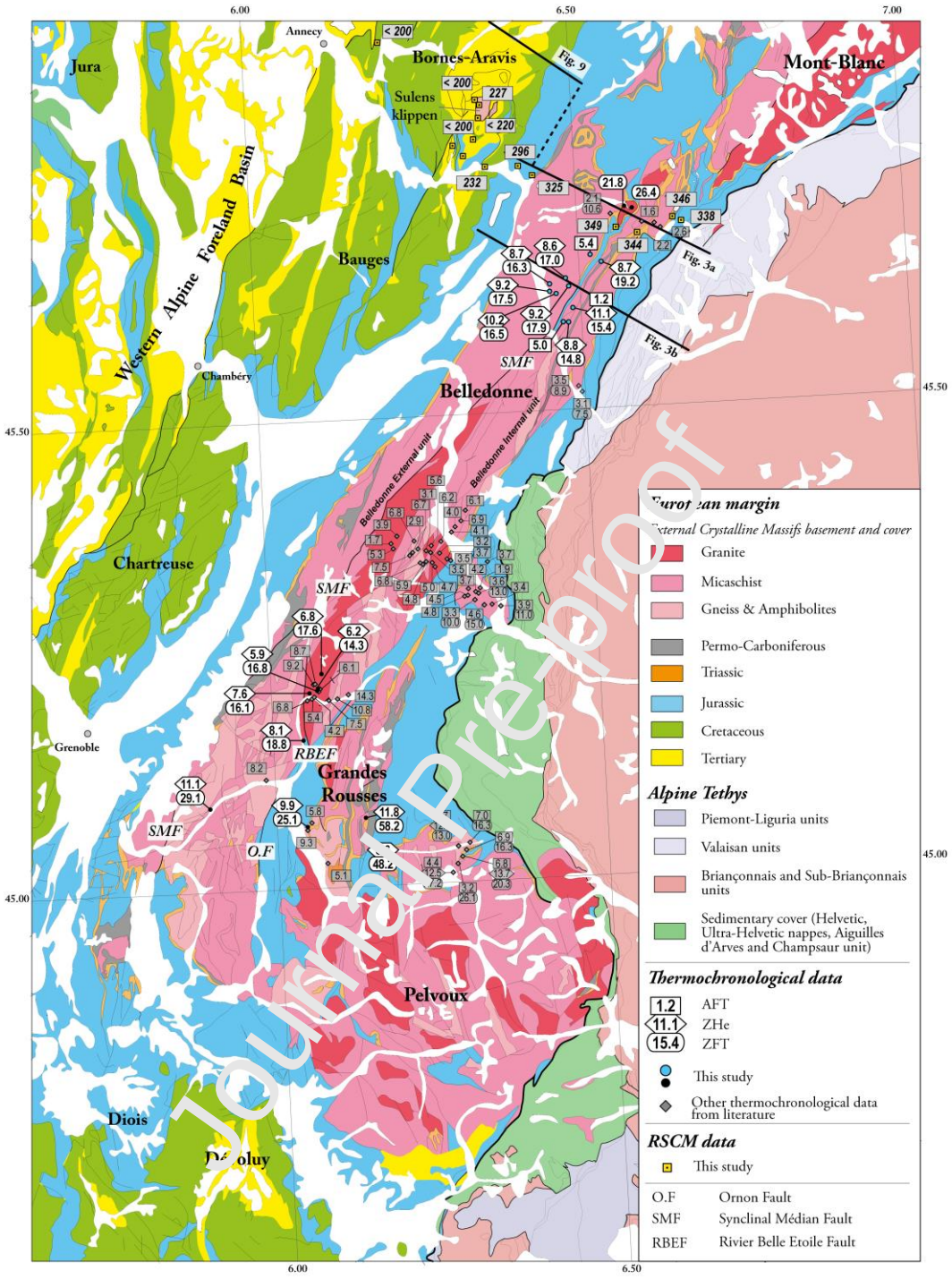

Figure 2: Geological map of the Belledonne, Grandes Rousses and Pelvoux massifs with thermochronological data from this study (Blue dots used in Figure 3 and black dots) and literature (Grey diamond-shaped; North Belledonne: ZFT and AFT: Seward and Mancktelow, 1994; Fügenschuh and Schmidt, 2003. Central Belledonne: ZFT and AFT: Lelarge, 1993; Fügenschuh and Schmidt, 2003. South Belledonne: ZFT and AFT: Sabil 1995; Bernet et al.,

2001. Pelvoux: ZFT, ZHe and AFT: van der Beek et al., 2010). RSCM data are represented with yellow square and T_{MAX} temperatures in degrees.

2. Geological setting

2.1. The Alpine collision

The Western Alps resulted from subduction of the Ligurian Ocean since the Late Cretaceous, followed by continental subduction and collision of the European margin during Eocene and Oligo-Miocene times (e.g., Chopin, 1987; Stampfli et al., 2002; Bucher et al., 2004; Ceriani & Schmid, 2004; Dumont et al., 2012). Continental collision between the European proximal margin and the proto-orogenic wedge (constituted by a nappe stack of Briançonnais/Ligurian/Austroalpine units) led to crustal thickening in the External Zone (e.g., Burkhard and Sommaruga, 1998; Leloup et al., 2005; Dumont et al., 2008; Sanchez et al., 2011; Bellahsen et al., 2012 ; Herwegh et al., 2020), resulting in the deformation of the ECMs, the initiation of crustal ramps and the subalpine belts during Oligo-Miocene times (**Fig. 1**) (e.g., Bellahsen et al., 2014) and the attainment of greenschist facies metamorphic conditions (e.g., Gratier et al., 1973; Rolland et al., 2003; Challandes et al., 2008; Sanchez et al., 2011 Cenki-Tok et al., 2014; Egli et al., 2016, 2017). Finally, the Miocene activity of frontal crustal thrusts (Bellahsen et al., 2012, 2014; Bellanger et al., 2014, 2015; Boutoux et al., 2016; Girault et al., 2020) combined with erosion led to exhumation of the ECMs.

2.2. The External Crystalline Massifs

The ECMs consist from north to south of the Aar, Aiguilles Rouges and Mont Blanc, Belledonne, Grandes Rousses and Pelvoux and Argentera massifs (**Fig. 1**). Their Triassic to Early Cenozoic sedimentary cover, in which several asymmetric syn-rift basins of Liassic to Dogger age are preserved (e.g. Lemoine and al., 1986), was also shortened (e.g., Lemoine et

al., 1986; Burkhard and Sommaruga, 1998; Bellahsen et al., 2012; Bauville et Schmalholz, 2015; Boutoux et al., 2016; Lafosse et al., 2016; Kiss et al., 2020; **Figs. 1 and 2**).

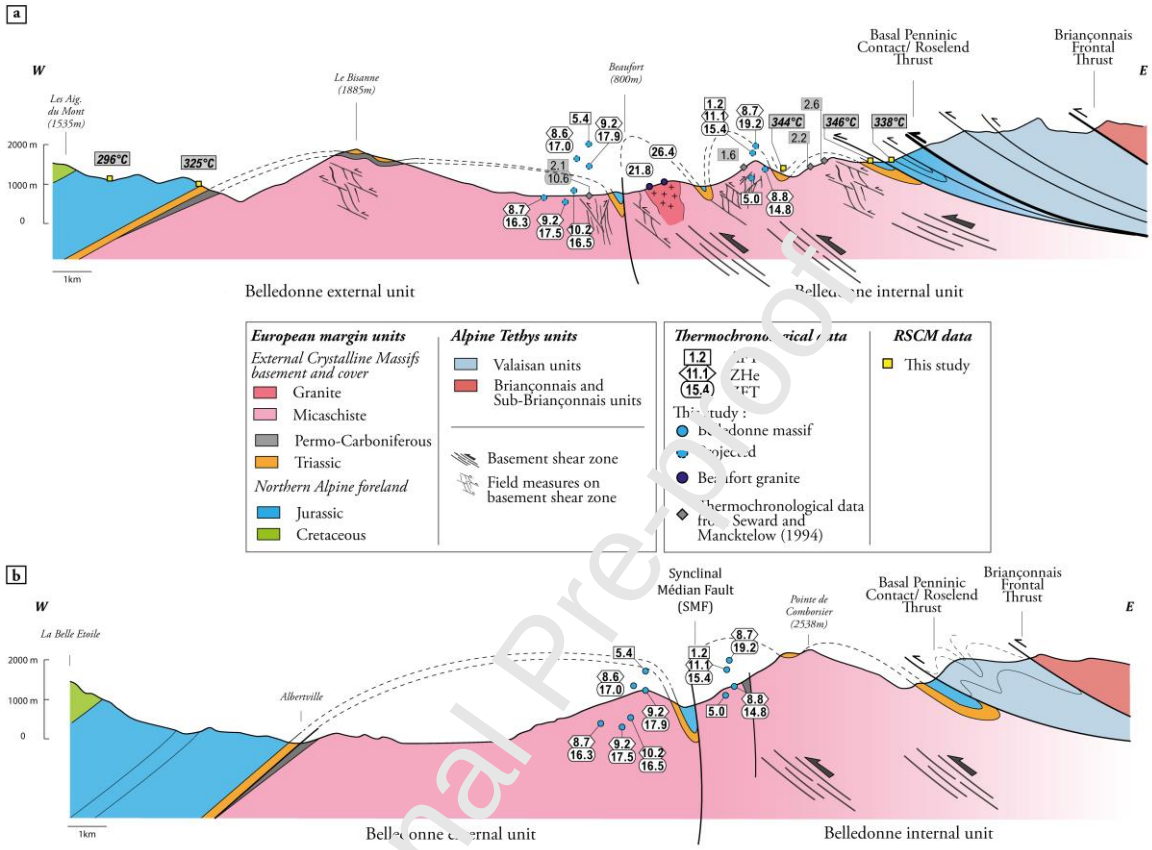

Figure 3: Cross section of (a) the Beaufort massif and (b) the Belledonne massif. The location of the cross section is shown in Figs. 1 and 2. Cross-section (a) displays projected LT thermochronological data (dashed blue circle).

The ECMs consist of various early Paleozoic metamorphic, plutonic and migmatitic rocks (e.g., von Raumer, 1984, 1998; von Raumer and Bussy, 2004), and late Paleozoic non-metamorphic sedimentary and volcanic series (**Figs. 1, 2 and 3**). In detail, the study area, i.e., the Belledonne (BD) and Grandes Rousses (GR) massifs, can be divided into different tectonic units delimited by strike-slip faults**,** namely the Synclinal Median dextral strike-slip

Fault (SMF) and the Rivier Belle Etoile Fault (RBEF) (**Figs. 2 and 3)** (e.g., Bordet and Bordet, 1963; Simeon, 1979; Bodelle and Goguel, 1980; Guillot and Ménot, 2009; Brillant et al., 2015; Fréville et al., 2018; Ballèvre et al., 2018).

The Belledonne massif can be separated into an external and an internal domain (**Figs. 2 and 3**), whose limit strikes west of the SMF. The external domain consists of medium metamorphic-grade micaschist series called the *Série Satinée* (Barfety et al., 1972, 2000; Ballèvre et al., 2018). In the internal domain (**Figs. 2 and 3**), the central unit, located between the SMF and RBEF, SW of the BD is characterized by a pre-Alpine nappe stack of late Devonian to Early Carboniferous age (Fernandez et al., 2002), including the Chamrousse Ophiolite, amphibolite facies metamorphic rocks, and the Visean volcano-sedimentary series (Menot, 1988; Barfety et al., 2000; Debon and Lemmet, 1999), dated at 332 ± 13 Ma (Sept-Laux granite; zircon U-Pb dating, Debon et al., 1994) and ca. 352 Ma (Rioupéroux unit; zircon U-Pb dating, Fréville et al., 2018). The eastern part of the internal domain (**Figs. 2 and 3**) consists of Variscan granites and migmatites with rare eclogitic relics (Bordet et Bordet, 1963; Paquette et al., 1989; Menot, 1988; Ballèvre et al., 2018; Fréville et al., 2018).

The GR and BD massifs are separated by an inherited Liassic half graben, named the Bourg d'Oisans half graben that is controlled by the Ornon fault (**Fig. 2**). The GR massif consists of different lithologic units including granites (i.e., Alpetta granite and Roche Noire – La Fare granite), carboniferous deposits, amphibolites, orthogneiss and migmatites (e.g., Bogdanoff et al., 1991; Debon and Lemmet, 1999) that are separated by N20-N30 striking faults.

Alpine P-T metamorphism recorded in the sedimentary cover of the GR massif is estimated to have reached temperatures between 320 °C and 350 °C (Bellanger et al., 2015) and pressures around 2.3 to 2.5 kbar, with a K/Ar age on phyllites of around 26.5 Ma +/- 0.2 Ma from the Dauphinois Lias of Bourg d'Oisans (Nziengui 1993). Furthermore, chlorite geo-thermometry

in the basement of the Pelvoux massif provided maximum Alpine temperatures between 240 and 300 °C interpreted as the temperature of shear zone activity between ca. 33 and 25 Ma (Simon-Labric et al., 2009; Bellanger et al., 2015). In the cover, the maximum temperature is apparently higher (RSCM data, 330 °C, see Bellanger et al., 2015 for a discussion). Cooling is constrained by paleomagnetic analyses with age/temperature couples between 24.1 Ma / 302 °C and 20.2 Ma / 182 °C (Crouzet et al., 1999, 2001) and by few AFT data indicating apparent cooling ages between 5.1 and 9.3 Ma (Sabil, 1995; **Figs. 2 and 3**).

Alpine P-T metamorphism is not well constrained in the BD massif but it is most likely similar to that of the GR massif. Alpine reverse shear zones with top-W and top-E shear sense were described and interpreted as Oligo-Miocene in age (Marquer et al., 2006). Cooling of the BD massif is constrained by LT thermochronological data with ZFT ages ranging in the northern part between 7.5 and 10.6 Ma (Fügenschuh and Schmid, 2003), and AFT ages ranging between 1.6 and 10.3 Ma (Lelarge, 1993; Seward and Mancktelow, 1994; Sabil 1995; Fügenschuh and Schmid, 2003; **Figs. 2 and 3**). Surface uplift of the BD massif can be attributed to the crustal ramp connected to the detachment bellow the massif (e.g., Philippe, 1995; Bellahsen et al., 2014).

2.3. Alpine Foreland Basin

We term the foreland as the whole of the foreland basin and the Subalpine chains. It comprises the Subalpine chains (Chartreuse, Bauges, Bornes-Aravis) and foreland basins which includes basins deformed in the Subalpine chains, and less deformed ones in a more external position, namely the North Alpine Foreland Basin (NAFB) from Geneva and beyond Zurich and the West Alpine Foreland Basin (WAFB) south of Geneva (**Figs. 1 and 2)** (e.g., Homewood et al., 1986; Sinclair, 1997; Allen et al. 1991; Sissingh, 2001, Ford et al., 2006).

The sedimentary succession of the NAFB and WAFB consists of four lithostratigraphic groups (Matter et al., 1980) and can be divided in two transgressive-regressive mega-sequences (e.g., Sinclair, 1997; Kempf et al., 1997, 1999; Kuhlemann and Kempf, 2002). The first mega-sequence comprises from bottom to top, the Lower Marine Molasse (UMM) and the Lower Freshwater Molasse (USM) deposited from the late-Rupelian to the late Aquitanian (i.e., 34-21 Ma). The base of this sequence corresponds to the flysch-to-molasse transition. The second mega-sequence consists of the Upper Marine Molasse (OMM) overlain by the Upper Freshwater Molasse (OSM) deposited from Upper Aquitanian to Serravalian times (i.e., 21-10 Ma) and corresponds to a filled to overfilled transition. Sedimentation in the foreland basin continued up to ca. 10-5 Ma.

During Oligocene-Miocene times, thrusting within ECM basement led to crustal thickening along the ECM belt and caused the deformation of a peripheral foreland basin and the Subalpine Chains through a series of several deformation stages. First, a sub-briançonnais nappe (Sulens klippen; **Fig. 2**) was thrusted over the Bornes massif and on to the NAFB (Préalpes sub-briançonnais and briançonnais nappes). Second, during the Burdigalian, the subalpine fold-and-thrust-belt initiated above their decollement, activated by crustal ramps rooted below the ECMs and then propagated underneath the molasse basins along Triassic evaporite layers and deformed the NAFB and WAFB basins (Becker, 2000; Bellahsen et al., 2014; Burkhard and Sommaruga, 1998; Deville and Sassi, 2006; Gorin et al., 1993; Laubscher 1961). Similarly, during late Miocene times the Jura fold-and-thrust-belt was formed (Becker, 2000; Looser et al., 2021). Finally, Pliocene uplift (Cederbom et al., 2004, 2011) resulted in erosion of the NAFB.

3. Methodology

Nineteen samples were collected for LT thermochronology analyses (zircon and apatite fission-tracks and zircon (U-Th-Sm)/He in the BD and GR massifs, along 3 vertical profiles

(**Figs. 2, 3** and **Table 1**). Eight samples were collected in the northern part of the BD massif (three samples from the internal part and five samples from the external part). Six samples were collected in the southern part of the BD massif, and three samples in the GR massif (**Figs. 2, 3** and **Table 1**). In each vertical profile the horizontal distance between all samples is less than 2,5 km except for BD-17-16 and BD-17-02 which are, respectively, at 5 km and 5,5 km horizontal distance from the other samples, and no fault is mapped between the samples.

Apatites and zircons were separated from bulk rock after crushing, sieving (75-250 µm fraction) and shaking table concentration, and using standard heavy-liquid density and magnetic separation techniques in CRPG (Nancy, France) and ISTerre (Grenoble, France).

Furthermore, 14 samples for RSCM thermometry analysis were collected from the Jurassic to Eocene metasedimentary cover of the northern part of the BD massif (**Figs. 2, 3** and **Table 2**).

3.1. Raman spectroscopy on carbonaceous material

The sampled metasedimentary rocks contain some carbonaceous material (CM), which permits the assessment of the maximum temperatures attained by these rocks during metamorphism. During burial temperatures increase and organic matter is progressively transformed into graphite. This process is irreversible and thus records the maximum temperature (T_{MAX}) experienced by the rock (Beyssac et al., 2002a, 2002b). The RSCM method is based on the quantitative determination of the degree of graphitization of carbonaceous material, measured from Raman Spectra (RS). In a spectral window, the RS can be divided into a graphite band (G) and several defect bands (D1, D2, D3, D4). The relative area of these bands reflects the degree of graphitization (see Beyssac et al. 2003 and references therein). Beyssac et al. (2002b) proposed an empirical thermometer, which links the R2 parameter defined as the relative area of the main defect bands (R2 = D1/(G + D1 + D2)) to T_{MAX} for a temperature range of 330 °C to 640 °C with an intrinsic calibration error of ± 50 °C and relative uncertainties on temperature in the range of 10-15 °C (Beyssac et al.,

2004). At lower temperatures in the range of 220–330 °C, Lahfid et al. (2010**)** estimate T_{MAX} by using the RA1 parameter (RA1 = (D1 + D4)/(G + D1 + D2 + D3 + D4)), with an intrinsic calibration error of ± 25 °C (Lahfid et al., 2010). Below 220°C, the temperature is poorly defined by these authors, therefore we do not display the absolute T value of samples whose calculated T lies below 220° C, and we only show that they are < 220 °C.

We used a Renishaw InVIA Reflex microspectrometer (IMPMC, Paris) with a 514.5 nm DPSS Cobolt laser in circular polarization for data acquisition. Focus on the sample was done using a DMLM Leica microscope with a 100x objective (NA = 0.85) yielding a spot size of ~ 1 μm and measurements were performed on polished thin sections, following the analytical procedures described in Beyssac et al. (2002b, 2003) and Lahfid et al. (2010). For each sample, 15–20 spectra were generally recorded and then processed using the software Peakfit 3.0 (Jandel Scientific). As the sampled rocks experienced peak temperature in the overlap range of the two calibration ranges described above, T_{MAX} was determined for each sample from the mean peak ratio (R2 or RA1) with the procedure giving the best fit.

3.2. Apatite and zircon fission-track analysis

Apatite and zircon grains were hand-picked and analysed at the Geo-thermochronology laboratory of ISTerre (Université Grenoble Alpes, France). Zircon aliquots were mounted in Teflon sheets, polished and etched with NaOH-HOH at 228 °C between 9 to 36 hours. Apatite aliquots were mounted in epoxy resin, polished and etched with 5.5 M HNO_3 for 20 sec. at 21 °C. Grain mounts of both mineral aliquots were covered with muscovite sheets as external detectors (Gleadow et al., 1976) and irradiated together with dosimeter glasses IRMM 540R for apatite and IRMM 541 for zircon at the FRM II Research Reactor in Munich (Germany) along with Durango and Fish Canyon Tuff standards. After irradiation, all white mica detectors were etched in 48% hydrofluoric acid at 21 °C for 18 min. Fission tracks were

counted at ISTerre using Olympus BH2 (zircon) and BX51 (apatite) optical microscopes at 1250x magnification with an FTStage 4.04 system (Dumitru, 1993). Zeta factors (Hurford and Green, 1983) were used in order to obtain individual fission-track ages. Central ages (Galbraith and Laslett, 1993) were calculated using the RadialPlotter program of Vermeesch (2009).

3.3. (U-Th-Sm)/He on Zircon

Zircons were hand-picked and analysed at CRPG (Nancy, France). Two to five single-grains were selected for analysis according to the following conditions: (i) prismatic to round shape, (ii) bipyramidal shape, unbroken and fracture free (when possible), (iii) equivalent spherical radius (length, width and thickness) > 60µm, and (iv) inclusion free (when possible).

Single-grain zircons were loaded in Platinum capsules for He extraction and outgassed at 1500 °C for 20 min by UV-laser. ^{4}He concentrations were determined using quadrupole mass spectrometry by isotope dilution (^{3}He spike). After He extraction, degassed zircon aliquots were retrieved, and contents of Uranium, Thorium and Samarium are measured at the SARM (CRPG, Nancy – France) following the Tibari et al. (2016) procedure. Zircon ages were corrected for α ejection (see Ketcham et al., 2011 and references therein). FCT zircon standard measured with this procedure displays a mean age of 28.3 Ma, with an external reproducibility of 8 % (1sigma).

3.4. Structural analysis and interpretation of seismic sections

We present a new large-scale cross-section from ECM to the Jura and discuss the relationships between exhumation of the basement massifs and dynamics of the foreland basin, we present and interpret a seismic section with associated well data. These allow us to define the geometries of sedimentary units and tecto-sedimentary interactions that occurred in

front of the ECMs during their main exhumation stage. This cross-section is completed by local fieldwork observations and structural measurements done on the Belledonne basement.

4. Results

4.1. Structural analysis

The external Belledonne unit (**Fig. 2**) shows a single antiformal basement structure, whereas the internal unit is deformed by several smaller-scale antiforms. The basement/cover contact of the internal unit is folded by tight folds. A schistosity, subparallel to folds axial surfaces affects the basement and is often associated to top-to-the-west shear senses and ~N110°E stretching lineations. The style of folding is more open in the external domain and the schistosity less developed there (**Fig. 3a**). Major faults (e.g., Synclinal Médian Fault, Rivière Belle Etoile fault; **Figs. 2 and 3**) are present.

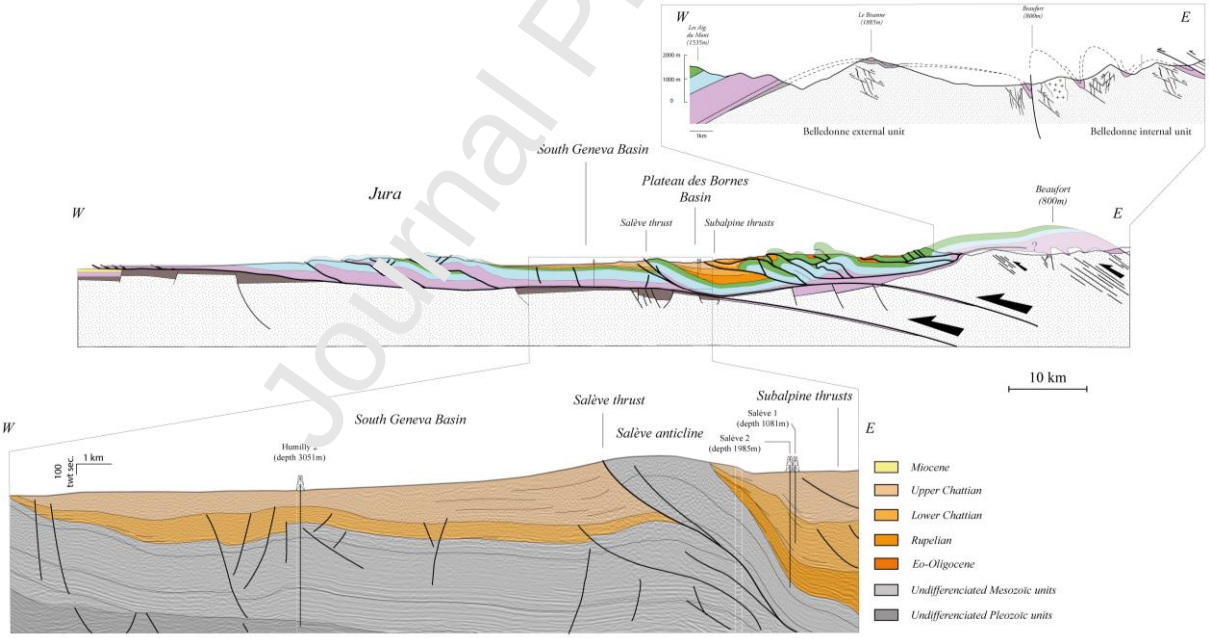

Figure 4: Cross section of the western Alpine collisional wedge, from the Belledonne basement through the molasse basin and Jura mountains. Cross section is redrawn and modified after Bellahsen et al. (2014). Basement cross section is from Fig. 3a. Interpretation of the Tertiary deposits of seismic line 88SVO-07 is from our study and pre-tertiary deposits

are from GeoMol project (GeoMol Team, 2015). Depth is in second two-way time (twt). See Fig. 1 for location.

Our new interpretation of a seismic line and well data across the Salève, the Plateau des Bornes Basin (i.e., Saleve 1 and 2 borehole) and the South Geneva Basin (i.e., Humilly 2 borehole, Charollais et al., 2007) is integrated to a crustal cross section (**Fig. 4**). The new interpretation shows the structure of the tertiary filling from Rupelian to Chattian (**Fig. 4**). Rupelian sediments are only found on the Plateau des Bornes basin (east of the Salève; **Fig. 2**), whereas Chattian deposits are found on both sides of the Salève (**Fig. 4**). Furthermore, in the Plateau des Bornes basin, sedimentary structures show progressive onlap towards the West from the Rupelian to the Chattian (**Fig. 4**). In the South Geneva basin, sedimentary wedges in the frontal part of the Salève ridge characterize the Upper Chattian deposits (Charollais et al., 2007). These sedimentary structures suggest that local subsidence during Chattian times (USM) was controlled by both the Subalpine and Salève thrusts (**Fig. 4**).

4.2. RSCM data

The RSCM results indicate T_{MAX} between < 200 °C and 349 °C. In detail, T_{MAX} ranges between 338 to 346 °C in the autochthonous cover of the BD massif and between < 200 °C and 325 °C further west in the Subalpine chains (Bornes massif) (**Figs. 2 and 3**). These data are in line with the presence of a sub-briançonnais nappe (Annes and Sulens klippen) overlying the ECM and their cover, thus increasing temperatures to around 300 to 350°C.

Figure 5: Age/elevation distribution of the thermochronological data (AFT, ZHe and ZFT) from (a) North External Belledonne (dark blue dots), (b) North Internal Belledonne (light blue dots), (c) South Belledonne (yellow dots) and (d) Grandes Rousses (purple dots). South Belledonne: AFT data from Sabil (1995). One elevation range of LT thermochronological data was selected (between 800m and 1400m) with, when possible, ZFT, ZHe and AFT data for thermal inversion modelling. Additional thermochronological data (AFT, ZHe and ZFT) at ~ 1800m were selected and used for thermal inversion modelling (see supplemental data 1).

4.3. Thermochronological data

Zircon fission-track results

ZFT ages in the North Belledonne are between 16.3 and 17.9 Ma (**Figs. 2, 3 and 5a; Table 2**) in external unit, and between 14.8 and 19.2 Ma in the internal unit, showing a positive age-elevation relationship (**Figs. 2, 3 and 5b; Table 2**). ZFT ages from the South Belledonne massif are in the range of 14.3 to 29.1 Ma and no obvious age-elevation relationship is detected (**Figs. 2, 3 and 5c; Table 2**). Finally, two samples from the Beaufort granite (Fig. 2 and 3a, east of Beaufort) display ZFT ages of 21.8 and 26.4 Ma (**Figs. 2 and 3**). ZFT ages in the GR massif are much older, between 25.1 to 58.2 Ma with a positive age-elevation trend (**Fig. 2, 3 and 5d; Table 2**).

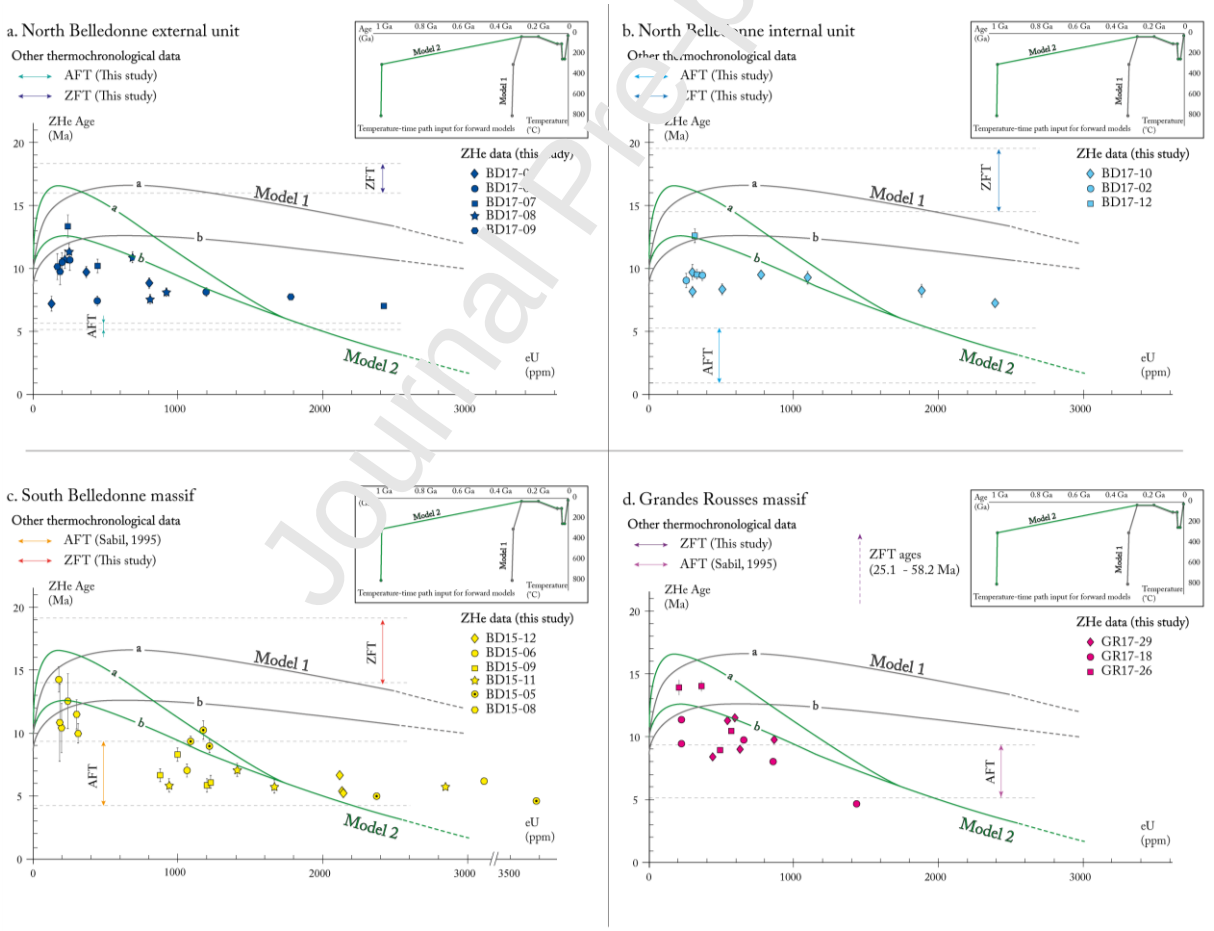

Figure 6: Age/eU distribution of the ZHe data with forward model curves assuming two different geological inputs: Model 1 and 2 (see inset). (a) North Belledonne external unit, (b)

North Belledonne internal unit, (c) South Belledonne massif and (d) Grandes Rousses massif. Arrows represent AFT and ZFT ages from this study and from Sabil (1995) for South Belledonne. (aside from AFT data on South Belledonne from Sabil, 1995). See supplemental data for the full range figure for Grandes Rousses massif. For the exhumation (see inset), we simulated two distinct scenarios using fission tracks data from this study (Fig. 5 and Tables 2 and 3) starting at 20 Ma (a) and 15 Ma (b) respectively and crossing the AFT closure temperature at 6 Ma (mean AFT ages of BD massif). The average size (75 μm) of zircon grains radius has been used in the model, as well as surface temperature of 10 °C.

Apatite fission-track results

Only three AFT samples from the Belledonne massif were analysed, which yield ages between 1.2 and 5.4 Ma (**Figs. 2, 3, 5a and 5b; Table 3**).

(U-Th-Sm)/He results

ZHe ages were determined from 17 samples that were also used for FT dating (**Figs. 5 and 6; Table 4**). Ages from the North BD internal unit range between 7.2 and 12.6 Ma and ages from the North BD external unit range between 7.2 and 13.4 Ma (**Figs. 2, 3, 5a and 5b; Table 4**). In the South BD massif they are between 4.7 and 14.3 Ma, whereas ages from the GR massif are in the range between 4.6 and 14.0 Ma (**Figs. 2, 3, 5c and 5d; Table 4**).

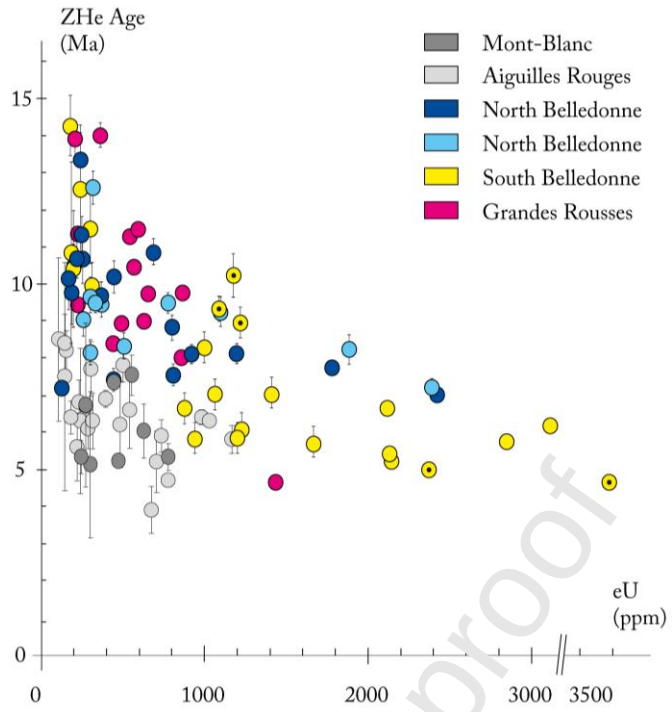

Figure 7: Age/eU distribution of the ZHe ages available for Aiguilles Rouges and Mont-Blanc massifs (Boutoux et al., 2016): grey circles, and ZHe ages from this study. Yellow circles with dark dots are zircons from sample BD15-05 from the south BD massif.

Overall these samples display ZHe ages ranging between those of AFT and ZFT of the same samples or of samples located in the same area (**Fig. 6**). However, for the southern BD and GR massifs, the youngest ZHe ages are similar or slightly younger than the AFT ages from the literature (Sabil, 1985). Despite this rather restricted range of ages, a negative correlation of ZHe ages vs. eU for individual samples and for samples from the same massif can be assessed (**Fig. 6 and 7**). In this correlation, ZHe ages with eU concentrations lower than 1000 ppm exhibit ages between 8 and 14 Ma, whereas most of ZHe ages with eU higher than 1000 ppm are in the range 5 - 9 Ma. For ages with eU < 1000 ppm, it seems that the oldest ages (12 - 14 Ma) are restricted to the eU range of 170 - 360 ppm. Except for sample BD15-05 (from south BD, Fig. 6c), a general tendency for high eU ages (> 1000 ppm, Fig. 6c) from south BD and GR to be slightly younger (5-7 Ma) than the ones from north BD (7 – 9 Ma) is observed.

4.4. Forward and inverse modelling of thermochronological data

Recent studies have shown that numerical modelling integrating apatite and zircon radiation-damage for (U-Th)/He systems (RDAAM models of Flowers et al., 2009 for apatite and Gunthner et al., 2013 for zircon) could provide valuable constraints for understanding, interpreting and determining a Temperature-time (T-t) path (e.g., Ternois et al., 2019; Anderson et al., 2017; Guenthner et al., 2014, 2015, 2017; Johnson et al., 2017; Powell et al., 2016) especially if they are coupled with fission track data (Vacherat et al., 2014, 2016; Boutoux et al. 2016; Bosch et al., 2016). However, some of these studies (Johnson et al., 2017; Vacherat et al., 2014; Gautheron et al., 2020) pointed out that the Zircon RDAAM model used to calibrate the HeFty or QtQT softwares (i.e. Guenthner et al., 2013) does not correctly reproduce the dependency of He diffusion to the accumulated dose of damages. Gautheron et al. (2020) investigated recently this potentiality using ZHe data published for Hercynian granites from the Pyrenean range (Bosch et al., 2016; Vacherat et al., 2016) and proposed that actual maximum He retentivity between positive and negative correlations does not occur at 2 x 10^{18} alpha/g (Guenthner et al., 2013) but significantly lower between 2 - 5 x 10^{17} alpha/g, close to the no-chain alpha recoil percolation level calculated by Ketcham et al. (2013).

In order to constrain our T-t paths, we performed both forward and inverse modelling using the HeFTy v.1.8.0 program (Ketcham, 2005). Forward modelling is first performed to discuss the control of the effective Uranium content (eU) on the ZHe age and the validity of the diffusion model implemented currently in HeFTy. In light of this test and associated potential limitations, inverse modelling is performed in a second step to determine T-t paths for the BD and GR massifs with the new ZFT, ZHe, AFT and RSCM dataset combined to LT thermochronological data available in the literature. Altogether, these data document T-t histories of both ECMs in the temperature range between 95 and 350 °C, whose lower bound

is defined by the AFT partial retention zone (Gallagher et al. 1998) and the upper one by T_{MAX} from RSCM data from this study.

Forward modelling of Zircon (U-Th)/He ages

The negative correlation with eU observed for ZHe ages (**Fig. 6 and 7**) is consistent with a multichronometric interpretation characterized by older ages at low-eU (i.e. low-damages), controlled by higher retentivity than the younger ages at high-eU (i.e. high-damage) (Guenthner et al., 2013; Vacherat et al., 2014; Johnson et al., 2017; Powel et al., 2016). In this framework, it would theoretically be possible to observe positive correlations associated to lower eU on the other side of a potential maximum retentivity threshold. It is not possible however to distinguish such a positive correlation in our dataset (**Fig. 6**), either because (i) it would occur at lower eU than the range documented in the measured samples (i.e. below 170 ppm) or (ii) because it occurs in a very restricted range of eU (between 170 and 250 ppm) and is consequently too steep to be documented precisely.

We used a forward modelling approach to try to reproduce such a potential dependence of ages to accumulated damage. Because Zircon RDAAM model calibration has been challenged recently (Johnson et al., 2017; Vacherat et al., 2014; Gautheron et al., 2020), the rationale here is to examine the way such models can (i) reproduce correctly the spread of ages for a single sample, and then validate the use of the population for the subsequent more precise multi-chronometric samples inversion, or (ii) highlight the same limitations as the one recognized by previous authors, and then rather require the use of a mean ZHe age for samples inversion. For this, we built a first model (Model 1 in **Fig. 6**) using the available and most robust data in the literature to constrain the T-t evolution of the considered massifs: (i) an age of ca. 335 Ma for the emplacement of the plutons of the massif (i.e., Granite des Sept-Laux at 332 - 335 Ma; Debon et al., 1994, 1998), (ii) a Liassic age of rifting (e.g., Lemoine et al., 1986), (iii) an Oligocene age of ca. 30 Ma for the youngest flysch deposits (Val d'Illiez

sandstone formation, 32 - 29 Ma, Sinclair, 1997), (iv) a T_{MAX} around 350 °C ± 25°C (Boutoux et al., 2016 and this study, based on RSCM data). For the exhumation, we simulated two distinct scenarios starting at 20 Ma (a on **Fig. 6**) and 15 Ma (b on **Fig. 6**), respectively (corresponding to the range of reset ZFT from BD massif). The average size of 75 µm of zircon grain radius as well as a surface temperature of 10 °C have been included in the model. Such model parameters which combine our ZFT data with realistic geological constraints should generate plausible range of ZHe age vs eU correlations at first order, at least to test the validity of model calibration, for which the position for the maximum of the ZHe values between positive and negative correlations is the critical point (see more detailed discussion in Gautheron et al., 2020).

On Figure 6, the curves obtained for Model 1a and b do not fit our data set, mostly because: (i) the maximum of retention between positive and negative correlations is simulated at a too high eU value (700 ppm), and (ii) the negative correlations of the model describe ages far too old than the ones observed in our data set for the high eU section (1000-3000 ppm). This conclusion is consistent with the proposition that the diffusion model implemented in HeFTy does not use a correct threshold for simulating rapidly increasing diffusivity after the maximum of retentivity (e.g. Gautheron et al., 2020). Some studies which explained their data with such RDAAM direct modelling considered very old initial protolith age in order to fit correctly the age vs eU correlations (Guenthner et al., 2015, 2017; Johnson et al., 2017; Powel et al., 2016). Using such old protolith ages tends to artificially increase the number of damages accumulated in the simulated grains, and therefore displaces the apparent maximum of retention in the models towards significantly lower eU values. In the case of our study (as in the case of the one conducted in the Pyrenees, Gautheron et al., 2020) the age of the protolith is very well known, and young (crystallization age of 335 Ma, Debon et al., 1994, 1998) which limits drastically the range of initial ages imputed in the RDAAM modelling. A

second unrealistic model using an age of 1 Ga for the initial protolith has been tested in order to examine its potentialities to fit the data by simulating a maximum of retentivity at lower eU. Results with such an artificial increase of the accumulated damages (Fig. 6, model 2) fit better the data and suggest that the ZHe age spread is indeed carrying a multichronometric message, but that our ability to model it is still non-operational in current modelling tools. This ZHe age spread could therefore only be interpreted semi-quantitatively with low eU cluster (~ maximum retention at 200 – 350 ppm, Fig. 7) corresponding to closure temperature of ~ 200 °C (slightly lower than the ZFT closure temperature), and high eU cluster (> 1000 ppm) corresponding to closure temperature close or equal to that of AFT.

Inverse modelling

As discussed above, the full range of single-grain eU-dependent ZHe ages cannot be simulated correctly with the diffusion model implemented in HeFTy. The discrepancy between model calibration and multichronometric natural ZHe data sets, like the one described above, is not compatible with a standard use of the modelling tool, which in such case outputs an extremely limited number of solutions. In order to keep the ZHe data associated to the FT data in the inverse modelling, we thus decided to compute representative mean aliquot ZHe ages and eU values for each sample. This allows us to overcome the previous complexity of the eU/ZHe-age curve modelling by averaging all parameters (ZHe, eU, closure temperature), which is consistent with (i) the systematic intermediate position of ZHe between ZFT and AFT ages, as well as (ii) the respective intermediate closure temperature of ZHe. To perform thermal inversions of the BD and GR massifs, we selected ZFT and ZHe coming from the same sample and AFT data at a similar elevation (between 800 m and 1400 m) as input for the inverse model (**Fig. 5 and supplemental data 1**). Additionally, high elevation inverse models can be found in the supplemental material (**see**

supplemental data 2). In order to obtain a complete and denser data set for the modelling of each transect, we completed our data with additional AFT data from the literature.

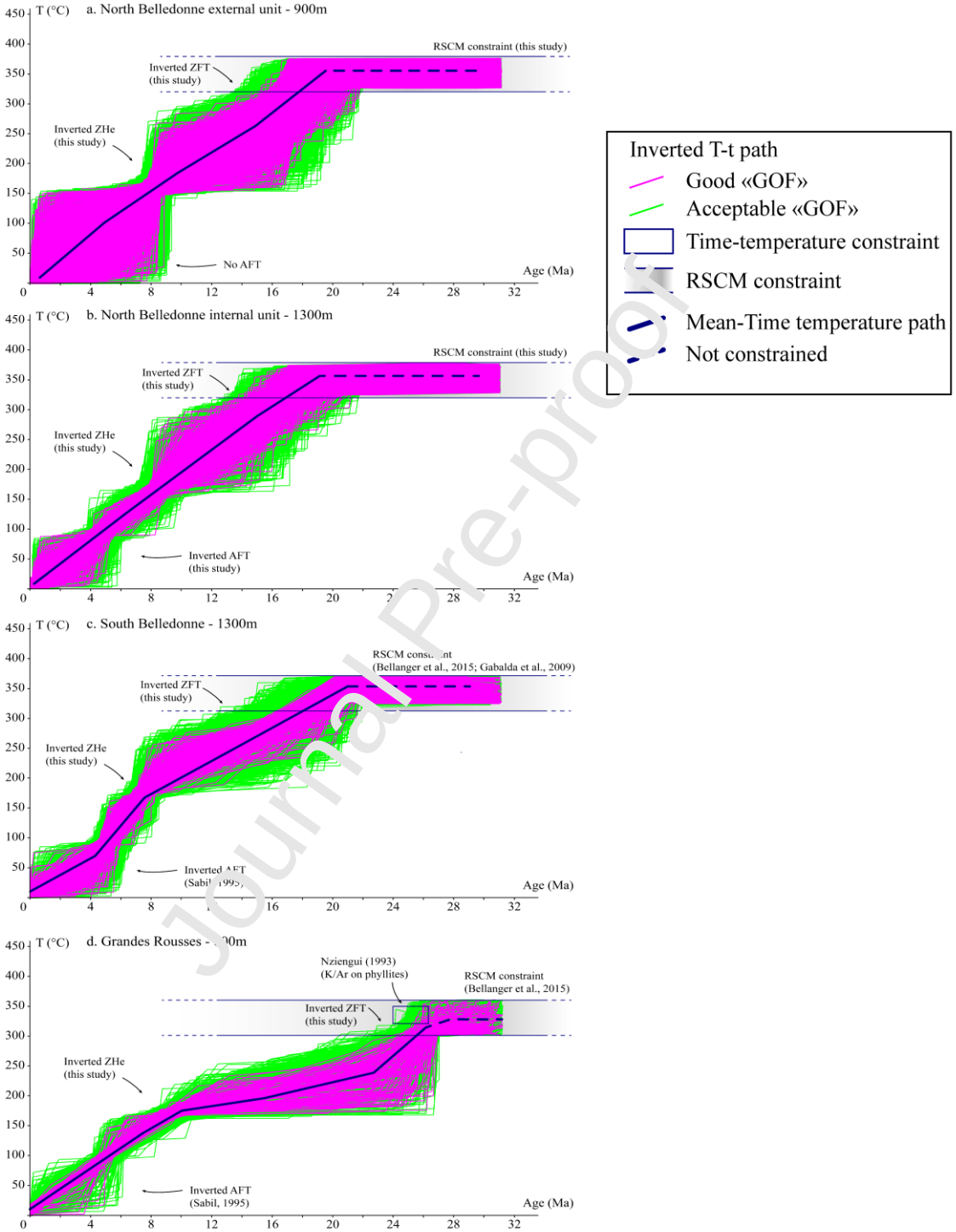

Figure 8: Thermal histories modelled with HeFTy software for the (a) North Belledonne external unit at 900m, (b) North Belledonne external unit at 1300m, (c) South Belledonne

massif at 1300m and (d) Grandes Rousses massif at 800m. T–t paths are statistically evaluated and categorized by their value of goodness of fit (GOF). 'Acceptable' results, in green, correspond to a 0.05 GOF value and 'good' results, in purple, correspond to 0.5 GOF (Ketcham, 2005) (see supplemental data 2 for thermal histories modelled with HeFTy software at higher elevation).

For the North BD external unit, we selected a sample at ~900 m elevation with ZFT and ZHe ages of 16.5 ± 2.6 Ma and 10.2 ± 0.6 Ma respectively (**Fig. 5a**). No AFT data exist there. For the North BD internal unit, we chose a sample located at ~1400 m for ZFT and ZHe, and AFT at ~1100 m to obtain a thermochronologic data triplet with ZFT, ZHe and AFT ages of 14.3 ± 2.2 Ma, 8.8 Ma ± 0.4 Ma, and 1.2 ± 2.4 Ma, respectively (**Fig. 5b**). For the south BD massif, we selected a sample at ~1200 m with ZFT age of 16.1 ± 2.0 Ma and ZHe mean age of 7.6 Ma ± 0.4 Ma, combined with AFT data from Sabil (1995) at 1250 m of 4.2 Ma ± 1 Ma (**Fig. 5c**). Finally, for GR massif at ~800 m, ZFT and ZHe ages from the same sample are respectively of 25.1 Ma ± 2.6 Ma and 9.9 Ma ± 0.6 Ma, and are associated with AFT data from Sabil (1995) of 5.1 Ma ± 1.0 Ma located at 755 m (**Fig. 5d**) and combined with K-Ar ages on white micas of the Lissie marly limestones from Bourg d'Oisans (Nziengui, 1993). Considering that T_{MAX} are around 350 °C ± 25°C for the ECMs sedimentary cover units (this study; Bellanger et al., 2015; Boutoux et al., 2016; Girault et al., 2020), we can assume that all AFT, ZHe and ZFT thermochronometers of the sampled rocks were reset during burial under the internal units. These T_{MAX} values are also included in the inverse modelling as a thermal constraint (**Fig. 8**).

Thus, in HeFTy, we selected a time frame only between the inferred age of the thermal peak and the present. The next step of the procedure consists in randomly testing 300,000 T–t paths for each model. T–t paths were statistically evaluated and categorized by their value of goodness of fit (GOF), calculated separately for the age data using the equation of Ketcham

(2005). All results are presented with several curves corresponding to 'Acceptable' results (with 0.05 GOF value), 'good' results (with 0.5 GOF value) and a mean T–t path (**Fig. 8**) (see Ketcham, 2005 and references therein). We modelled four sections: North BD external unit, North BD internal unit, south BD, and GR at low elevation (**Fig. 8**).

For both North BD models, we observe a similar trend as for all HeFTy models (**Figs. 8a and 8b**). However, only models with inverted AFT data are well constrained (**Fig. 8b**) for the late cooling (i.e. after 10 Ma). These models show overall a constant cooling rate (15 °C/Myr; **Figs. 8a and 8b**) between 17 and 4 Ma. For the South BD massif, the inverse model is slightly different than for the North BD massif, with an older onset of cooling, a cooling rate of 20 °C/Myr between 22 - 8 Ma, and an increase of cooling rate between 8 - 4 Ma to 25 °C/Myr; **Fig. 8c**), which is consistent with the fact that at high-eU the south BD ZHe ages cluster at about 5- 7 Ma (Figs. 6c and 7). Finally, the HeFTy model of the GR massif displays an older onset of cooling at ~26 Ma ± 1 Ma (constrained by older ZFT data) with rapid cooling from 26 Ma to 23 Ma of 25 °C/Myr; **Fig. 8d**), followed by slow cooling between 23 and 9 Ma at 5 °C/Myr; **Fig. 8d**), and finally rapid cooling since 9 Ma with 15 °C/Myr; **Fig. 8d**). Post 5 Ma cooling at low temperatures is not well constrained and remains hypothetical due to lack of AHe and $^{4}He/^{3}He$ data.

5. Discussion

5.1. Thermal peak

The range of RSCM T_{MAX} data obtained from the BD cover and Subalpine chains are in the range of <200 °C to 349 °C and they are consistent with RSCM temperatures obtained from the cover of the Mont Blanc and Aiguilles Rouges massifs (Boutoux et al., 2016), the Pelvoux and GR massifs (Bellanger et al., 2015), the eastern part of the Belledonne massif and Briançonnais (Gabalda et al., 2009), the Helvetic nappe complex (Nibourel et al., 2018;

Girault et al., 2020), and with the alpine metamorphic peak conditions estimated at about 320 °C to 370 °C for the GR sedimentary cover (Crouzet et al. 2001). These data display a similar trend with temperature decreasing from E to W (**Figs. 2 and 3**). Furthermore, our data are consistent with forward temperature models from vitrinite reflectance data (Deville and Sassi, 2006), showing a thermal peak at 250 ± 10 °C in the Subalpine chains (i.e., the Bornes massif). In the Bauges massif, forward thermal models provide a maximum burial temperature higher than 160 °C (Mangenot et al., 2019). The higher T_{MAX} values in the Bornes compared to the Bauges massif may be explained by the fact that the internal units were thrust over the Bornes, similarly to the the Préalpes, but not, or only to a minor degree over the Bornes (Deville and Sassi, 2006).

Assuming a normal geothermal gradient with T decreasing upward, the T_{MAX} of 349 ± 25 °C recorded in the cover rocks of the BD massif likely represents a lower boundary for the T_{MAX} of the underlying basement. The age of peak metamorphism in the BD massif is only poorly constrained based of dating quartz veins around 24 - 26.5 Ma (K-Ar, Demeulemeester et al 1986; Nziengui 1993). White micas $^{40}Ar/^{39}Ar$ ages of 14.5 ± 0.1 Ma in the northern BD massif correspond to a stage of recrystallization or neocrystallization during the activity of top-to-NW shear zones (Egli et al., 2017). In the Pelvoux massif, shear zones have been inferred to be active between 34 and 25 Ma ($^{40}Ar/^{39}Ar$ on white micas; Bellanger et al., 2015; Simon-Labric et al., 2009).

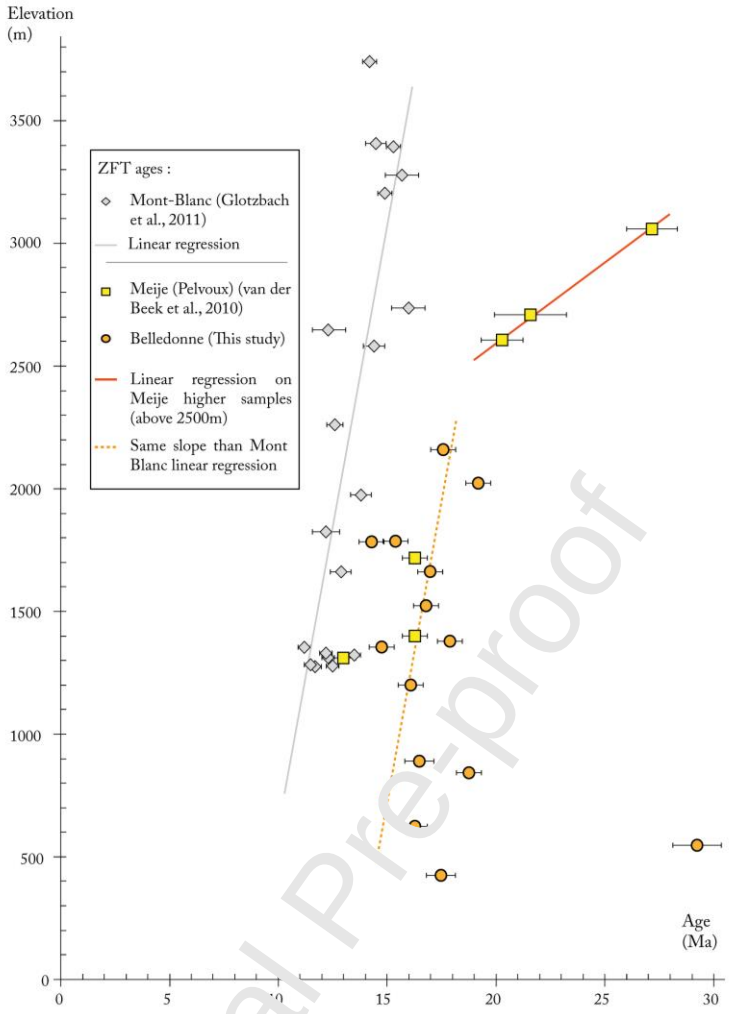

Figure 9: Age/elevation distribution of zircon fission-track (ZFT) ages (with 1σ error) available for Aiguilles Rouges (Soom, 1990) and Mont Blanc (Glotzbach et al., 2011): gray diamond-shaped, Belledonne (this study): orange circle, Pelvoux – Meije massifs (van der Beek et al., 2010): yellow square (see **supplemental data 3** for full figure display with Grandes Rousses)

5.2. Cooling/exhumation of the external Western Alps

With the new thermochronological data, we provide a new cooling sequence for the external zone. The cooling age must be taken as minimum values for exhumation as the latter may have started slightly before. However, the delay most probably did not exceed a few Myrs. Moreover, ages of exhumation can also be estimated from age/elevation diagrams.

The internal and external units of the northern BD massif have very similar Temperature-time (T-t) paths with an onset of cooling quite synchronous at ~18 Ma (**Figs. 8a and b**). Thus, the Synclinal Median fault (**Figs. 2 and 3a**) was not reactivated, or only by small displacements, during Alpine collision (at least not after 18 Ma), in line with previous interpretations (Bellahsen et al.; 2014; Boutoux et al.; 2016; Lafosse et al., 2016). In the southern BD massif, the onset of cooling is quite similar (~21 Ma ± 1 Ma; **Fig. 8c**) to the northern part. The T-t path of the GR massif is different from the Belledonne massif and it displays an older onset of cooling, at ~26 Ma (**Fig. 8d)**. This age is synchronous with the end of ductile basement deformation in the Pelvoux massif (25 Ma, Bellanger et al., 2015).

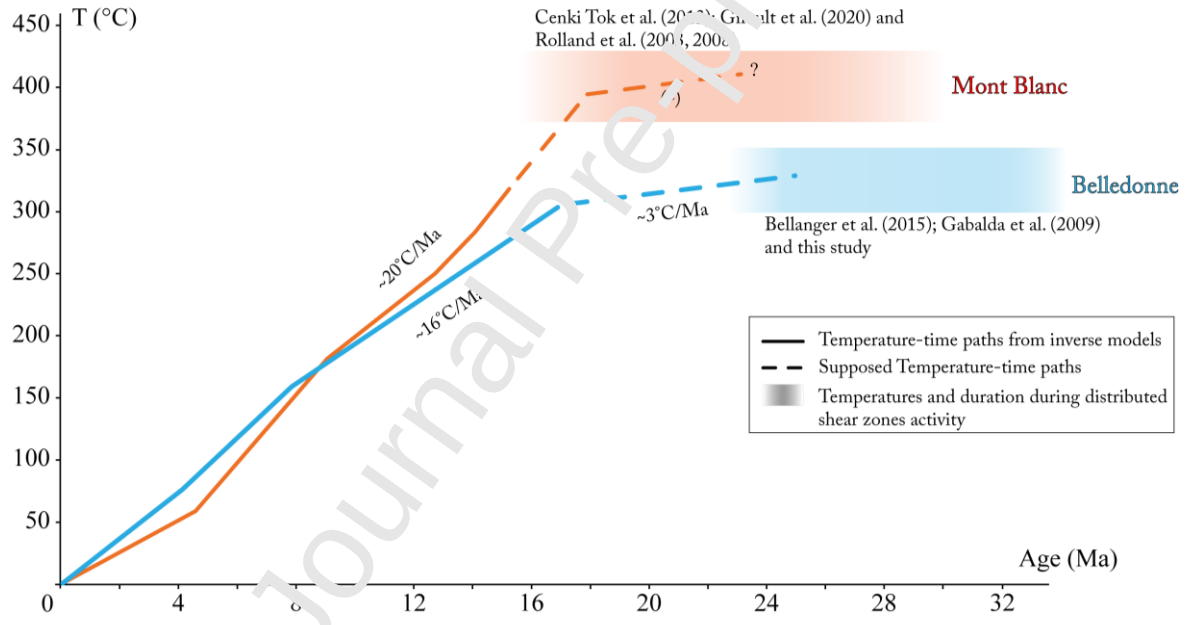

Figure 10: Temperature-time path for the Belledonne and Grandes Rousses massifs based on our HeFTy thermal modelling. Early cooling of Belledonne is drawn from Pelvoux highest ZFT ages (van der Beek et al., 2010). (*) Slow cooling for Mont Blanc massif is from sedimentological and detrital provenance data from Schlunegger et al. (1998), von Eynatten et al. (1999) and Spiegel et al. (2000).

At equivalent elevation (i.e., around 1500 m), ZFT ages from the Pelvoux massif (i.e., Meije transect from van der Beek, 2010; **Figs. 2 and 9; see supplemental data 3** for a larger scale) are similar to our ZFT ages of both the southern BD and the GR massif. The T_{MAX} data of the sedimentary cover of these massifs (Bellanger et al., 2015) is in the same range as those obtained for Belledonne massif (**Fig. 2**). In the Pelvoux massifs ZFT samples collected at an elevation higher than 2500 m show some ages distributed over a wider range, between 20 and 27 Ma (van der Beek et al., 2010; **Fig. 9**). Based on the compiled LT thermochronological data, we propose that an early phase of cooling for South Belledonne began at ca. 25-27 Ma, which is consistent with thermochronological and thermo-paleomagnetic data from the literature (Nziengui, 1993; Crouzet et al., 1999, 2001; see previous paragraph; **Figs. 8 and 10**). During this period, exhumation was slow within the BD and Pelvoux massifs with a ca. 50 m. $Myrs^{-1}$ rate based on ZFT ages (**Fig. 9**). This onset of cooling at 25-27 Ma corresponds to the end of shortening and thickening accommodated by distributed basement shear zones in the Pelvoux massif (25 Ma-27 Ma; Simon Labric et al., 2009; Bellanger et al., 2015).

Further south, the Argentera massif shows a cooling pattern similar to our observations in the southern BD, GR and Pelvoux massifs, with a metamorphic peak followed by slow cooling that started at 29 Ma (i.e., 8-5 °C/Myr; Bogdanoff et al., 2000; Bigot-Cormier, 2000; Sanchez et al., 2011; **see supplemental data 3** for complete compiled LT thermochronological data). We propose that the southern, external part of the Alpine arc, from the Belledonne to Argentera ECMs, is affected by nearly coeval onset of cooling in the Oligocene during the activity of basement shear zones.

In the northern ECMs (Aar, Aiguilles Rouges and Mont Blanc massifs), cooling started at least at 18 Ma (Challandes et al., 2008; Rolland et al., 2009; Weisenberger et al., 2012; Boutoux et al., 2016; Herwegh et al., 2019; Berger et al., 2020; this study) most likely due to the activation of frontal crustal ramps, implying surface uplift and erosion. However, we

cannot exclude an older onset of exhumation of the northern ECM's, the record of which would be found in samples eroded and deposited in the Molasse basin. Furthermore, an isothermal exhumation could also be considered since 22 Ma, as suggested by Herwegh et al. (2020), which would cannot be inferred from thermochronology without thermal-kinematic modelling (e.g. Braun et al. 2012).

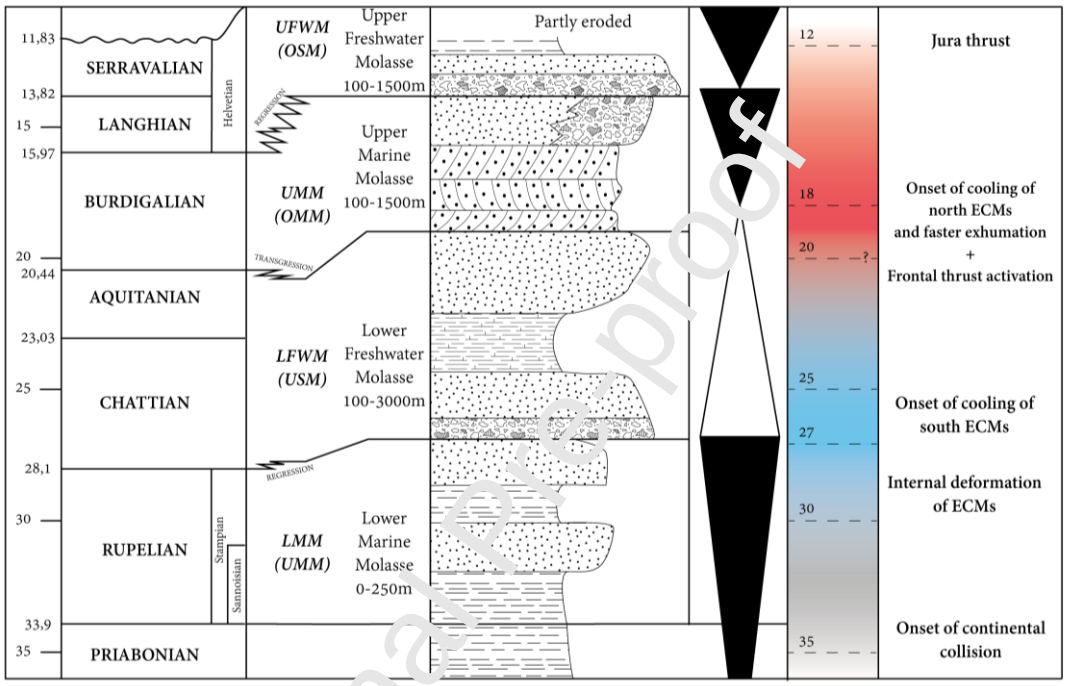

Figure 11: Tertiary stratigraphy, providing formation names and thicknesses used in the present work. The four lithostratigraphic groups (Matter et al., 1980) and the two transgressive-regressive mega-sequences (Sommaruga, 1997; Sinclair, 1997; Beck et al., 1998; Kuhlemann and Kempf, 2002) are presented in light of the tectonics events in the collisional wedge from this study.

Thus, to sum up, we show that there might be a diachronism between the exhumation of the northern, western and southern ECMs (**Fig. 11**). In the West, exhumation most likely started around 27 Ma at slow rates whereas in the North it started at least at 18 Ma or earlier, around 20-25 Ma (see in Herwegh et al., 2020; Schlunegger et al., 1998; von Eynatten et al., 1999;

Spiegel et al., 2000). We interpret this potential diachronism as being due to a time delay in the activation of the frontal ramps. This is in line with ages of shear zone activities within the ECMs, which are older in the Argentera and Pelvoux massifs compared to the Mont Blanc and Aar massifs (compare dataset in Rolland et al., 2008, 2009; Cenki-Tok et al., 2014; Rossi and Rolland, 2014; Bellanger et al., 2015, Boutoux et al., 2016; Egli et al., 2017; Herwegh et al., 2020).

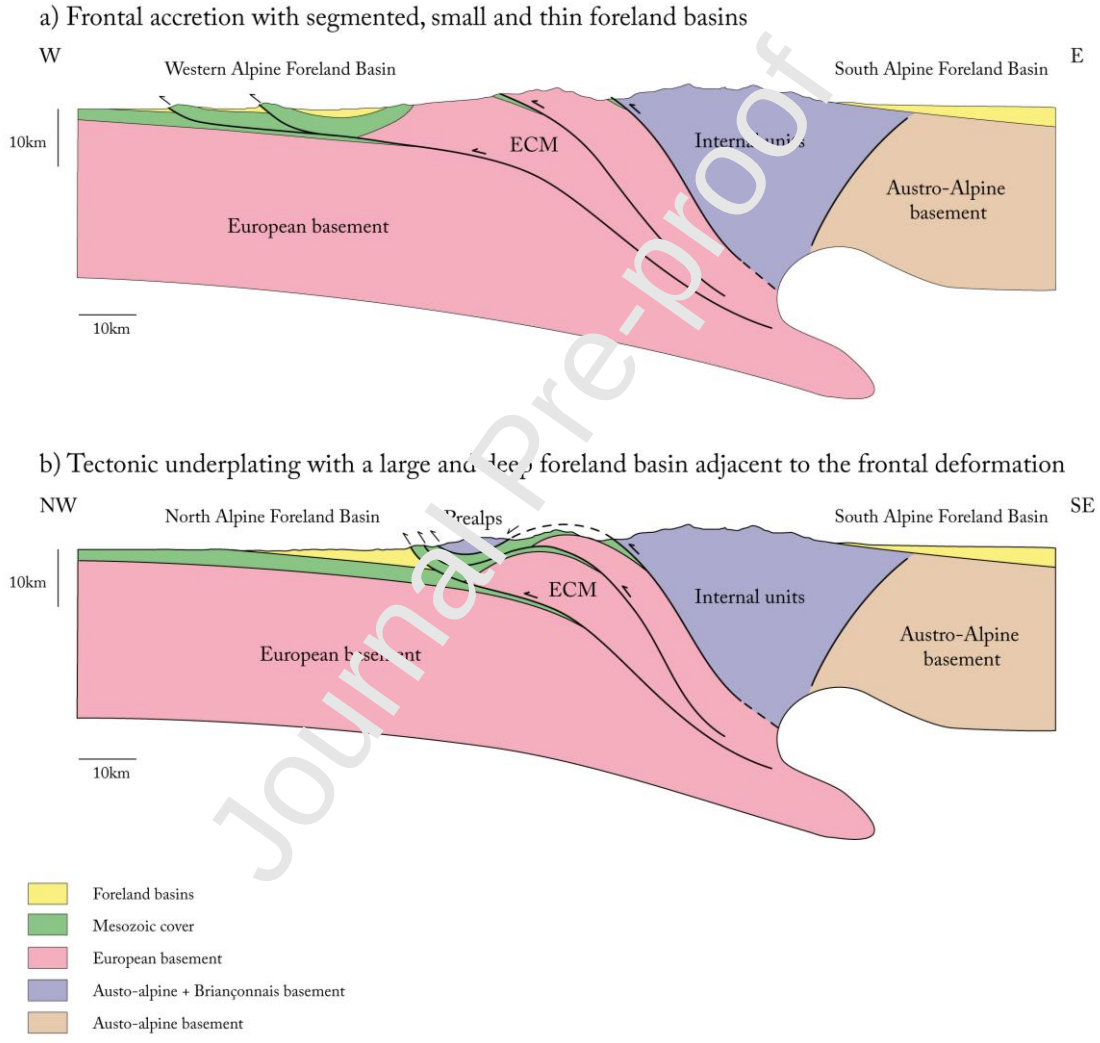

Figure 12: Simplified cross sections through a) the WAFB and the western Alpine collisional wedge and b) the NAFB and the northern Alpine collisional wedge redrawn and modified from Bellahsen et al. (2014).

In the West, collisional shortening in the external zone started slightly earlier (around 30-34 Ma, Simon-Labric et al., 2009; Bellanger et al., 2015) than in the North (around 30 Ma, Cenki-Tok et al., 2014) (**Fig. 11**). Moreover, this shortening is characterized by frontal accretion in the West (**Fig. 12**) with low shortening in the internal zone, while tectonic underplating is active in the northern external zone, with significant shortening in the internal zone (**Fig. 12**; Bellahsen et al., 2014; Rosenberg et al., 2015).

Beyond these differences in terms of style and possibly timing for the early history, since 18 Ma the northern and western ECMs show a similar, more rapid exhumation rate of ca. 500 m.Myrs^{-1} rate ± 40 m.Myrs^{-1} (**Fig. 9 and see supplemental data 3 for a larger scale**) and cooling rate between 16 and 20 °C/Ma (**Fig. 10**). This period also corresponds to a main event in the foreland basins (transition between mega-sequences, **Fig. 11**) as developed below.

5.3. Wedge exhumation and foreland sequences

Our results document the exhumation of ECM which is a major evolution of the wedge in western Alps and thus influence the evolution of the adjacent foreland basins. In order to test this influence, we discuss first order spatiotemporal relationship between ECM exhumation and the tectonic sequence and infilling of the WAFB.

During late Eocene to early Oligocene times, an underfilled flexural basin was developed ahead of the early collisional zone and was characterized by the deposition of turbiditic series such as the Annot, Taveyannaz, Val d'Illiez and Saint-Disdier sandstones (e.g., Meckel et al., 1996; Sinclair, 1997; Beck et al., 1998; Burkhard and Sommaruga, 1998; **Figs. 11**). Later sediment supply from the upper plate gradually increased as the orogen relief also increased (Bernet et al., 2009; Ford and Lickorish, 2004; Jourdan et al., 2012). The transition from the previous underfilled conditions to overfilled conditions is slightly diachronous along the

foreland basin (Sinclair, 1997) and occurred from early Rupelian (33.9 Ma) to middle-late Rupelian within the Lower Marine Molasse. At that time, all ECMs of the western Alpine arc attained their thermal peak, which was synchronous to distributed crustal shortening, as shown by dated ductile deformation in the European basement (e.g., Rolland et al., 2008; Simon Labric et al., 2009; Sanchez et al., 2011; Bellanger et al., 2015).

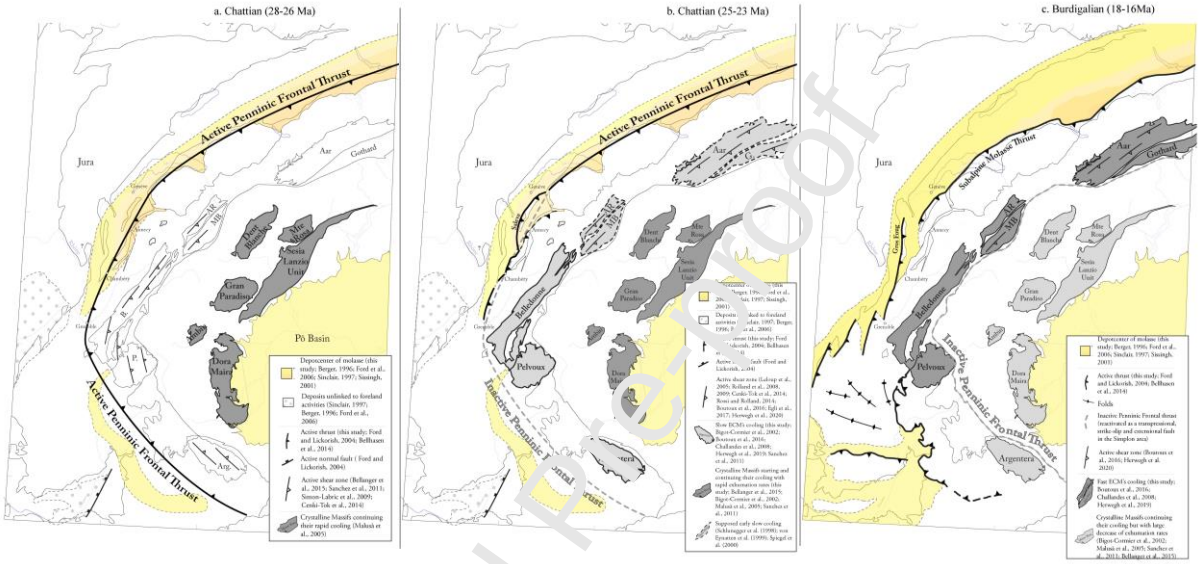

Figure 13: Exhumation map and sedimentary record of the western Alpine collisional wedge. (a) Early Chattian period during the molasse transition stage with a quite cylindrical foredeep shape (28-26 Ma), (b) Late Chattian period (25-23 Ma), (c) Burdigalian period with segmented molassic basin (18-16 Ma). This map was modified after Bousquet et al. (2012).

5.3.1. Early exhumation of ECM (28-18 Ma).

During deposition of the Lower Freshwater Molasse (ca. 28 - 18 Ma), the western ECMs (i.e., Pelvoux, Grandes Rousses and Belledonne) started to be exhumed, at around 25-27 Ma (**Figs. 9, 11 and 13a, b),** with a slow exhumation rate (**Fig. 9**) while the northern ECMs were still at their thermal peak (e.g., Boutoux et al., 2016).

The progressive onlap and growth strata within Chattian deposits in the Plateau des Bornes basin (**Fig. 4**) suggest that it was a piggy-back basin at around 25 Ma, hence during the initial stages of cooling of the western ECM basements (**Fig. 4**). At this time, subsidence of the basin most likely increased (Burkhard and Sommaruga, 1998), controlled by frontal thrusts (**Fig. 4**). During this period (i.e., Chattian - Aquitanian), the WAFB geometry changed from a quite cylindrical foredeep shape along the orogenic wedge (i.e. Eocene to early Oligocene times) to a segmented one, having distinct sub-basins (see also Berger et al., 2005; Charollais et al., 2007). While the NAFB was being filled by mega-alluvial fans (e.g., Sinclair and Allen, 1992; Berger, 1996; Schlunegger et al., 1997; Sinclair, 1997; Beck et al., 1998; **Figs. 11 and 13a, b**), the preserved WAFB display continental deposits showing distal river systems (Berger, 1996; Beck et al., 1998). Thus, the proximal part of the WAFB sedimentary system is probably not preserved. The orogenic wedge was progressively growing and delivered important sediment supply from main sources located in the Internal Zone (Mange-Rajetzky & Oberhansli, 1986; Mange-Rajetzky & Oberhänsli, 1982; Bernet et al., 2001; Jourdan et al., 2012; Fauquette et al., 2015).

The WAFB south of Chambery is less continuous and less documented (e.g., Ford et al., 2006), especially in the Vercors - Devoluy area (**Fig 13**). Surprisingly, only few evidences of Oligocene molassic basin between the ones of Devoluy and Savoy basin are preserved at the front of South Belledonne. A possible hypothesis for the absence of such deposits would be that such basin existed, but was later incorporated into the wedge and completely removed during the Miocene formation of the Vercors/Chartreuse fold-and-thrust-belt.

Alternatively, as the Pelvoux massif, and possibly, the Grandes Rousses and the South Belledonne massif started to be exhumed at 27-25 Ma, probably by activation of a crustal ramps at their base, also suggested by the unconformity at the base of the lower St-Disdier sandstones (Meckel et al., 1996). If such ramps initiated, it may have induced an early

formation of the fold-and-thrust-belt, although not evidenced yet, and no-, or only very small, Chattian - Aquitanian deposits. This would explain why only very scarce Chattian - Aquitanian deposits are observed below the Burdigalian ones (see in Kalifi et al., 2020).

Within the WAFB, including the Devoluy basin, deformation of the orogenic wedge was mainly accommodated by frontal basement accretion which led to small, thin and segmented molasse basins characterized by a pronounced west-directed migration (**Fig. 12a**). This is compatible with the amount of crustal shortening which is 2 or 3 times inferior in the west (Pelvoux and Belledonne massifs; Bellahsen et al., 2014 and references therein) compared to the north (Aar massif).

In the northern part of the Western Alps, the Penninic Thrust was active during the Chattian – Aquitanian (as shown by the Prealps overthrusting the NAFB Oligocene deposits and Ar-Ar ages on white micas, D_2 and D_3 events at 27-19 Ma in Cardello et al., 2019), and the Internal Crystalline Massifs (e.g., Gran Paradiso) and Austro-Alpine basement (e.g., Sesia) were still being exhumed, as shown by LT thermochronological data (see Malusà et al., 2005 and references therein) (**Fig. 13a, b**). Furthermore, the orogenic wedge was deformed mainly by basement unit underplating (e.g., Bukhard and Sommaruga, 1998) (**Fig. 12b**).

5.3.2. Faster exhumation of ECM (post-18 Ma)

This period corresponds to the onset of the second mega-sequence during which the ECMs cooled at higher rates in the West and in the North (**Figs. 9, 10, 11 and 13c**). It is noteworthy that this initial phase of exhumation was much slower and most probably characteristic of the transition between the distributed mode of shortening and the localized one. We propose that such transition ended at around 18 Ma and that true localized accretion started. Localized accretion with crustal ramps implies a more localized exhumation in the hanging wall ramps.

During the Burdigalian (20-16 Ma), the sea invades the WAFB and NAFB (Upper Marine Molasse) from the Gulf of Lion, migrating northward through the Valence graben (e.g., Rubino et al., 1990; Ford et al., 2004). Burdigalian deposits record a reactivation of subsidence combined with higher eustatic sea-level (e.g., Berger, 1996; Beck et al., 1998). Syn sedimentary flexure and thrusting is reported in WAFB during Burdigalian (Beck et al., 1998).

When the ECMs were incorporated into the collisional wedge, the foreland flexure and basin subsidence rates increased, resulting in westward migration, deepening and widening of the basin as recorded by Burdigalian deposits (Rubino et al., 1990; Kuhlemann and Kempf, 2002; Berger et al., 2005).

Thus, the generalized onset of rapid exhumation in the ECM (mainly w-verging structures as well as back-thrusting in the Mont Blanc and Aar massifs) and the related crustal ramps apparently controlled the first order sedimentary sequence of the molasse basin and may have facilitated the north-eastward migration of the Burdigalian marine transgression (**Figs. 11 and 13c**). Furthermore, the configuration of the flexural basin pursues to more segmented and individualized basins (**Fig. 13c**).

The rapid exhumation of ECM from 18 Ma is also probably providing a large sediment flux to the foreland. Deposition of Gilbert-type deltas at the front of the Chartreuse massif in the Chambery area (Kalifi et al., 2020) and conglomerates in the Voreppe area (Demarcq, 1962) attest for high sediment fluxes. Transition between Upper marine molasse and Upper fresh water molasse occurs around 16 Ma (Burdigalian - Langhian boundary) in Savoy basin may be a consequence of an increasing sediment flux from the ECM, not counterbalanced by subsidence.

6. Conclusion

Our new RSCM data show that the temperature peak reached by the BD cover units was close to 350 °C. Thermal modelling of our thermochronological data compiled with published data suggests that cooling initiated in the southern BD and GR massifs at around 27 Ma +/−1 Ma coevally with other ECMs located further south (Pelvoux and Argentera massifs). During this time, thrusts were active in the WAFB. Toward the North, in the northern BD massif, cooling started at 18 Ma +/−1 Ma coeval with other northern ECMs (Mont Blanc, Aiguilles Rouges and Aar massifs). At this time, exhumation was more rapid, possibly attesting for the activity of crustal ramps all around the Western Alps. Thickening and shortening of the internal and external zones controlled the flexural subsidence; evolution in the ECM is probably the main driver of the complex interplay between subsidence and sedimentary flux that is revealed by the main sedimentary sequences in the WAFB. Finally, differences in modes of tectonic accretion between underplating in the northern Western Alps and frontal accretion in the southern parts of the arc could explain the transition from a large (unique) molasse basin in the north to segmented small molasse basins in the west.

Acknowledgement

E. Delairis is thanked for thin section preparation. The authors acknowledge the help of O. Beyssac during RSCM data acquisition and for discussions. All the data and supplemental data presented in this paper can be found online (DOI: 10.6084/m9.figshare.14216912). This study was funded by CNRS INSU Syster program, BRGM RGF program, and ISTeP funds.

Supplementary material (DOI: 10.6084/m9.figshare.14216912)

Table 1: Raman spectroscopy of carbonaceous material data. GPS coordinates in WGS84 system, number of spectra (n), mean R2 ratio (Beyssac et al., 2002a) or RA1 ratio (Lahfid et al., 2010) reliant on best fit during post-processing using the software PeakFit following the methods described in Beyssac et al. (2002b) and Lahfid et al. (2010) with corresponding standard deviation, and calculated temperature with standard error (SE). Standard error is the standard deviation divided by √n. The absolute error on temperature is ±50 °C (Beyssac et al., 2002b). (a) Method from Lahfid et al. (2010) and (b) Method from Beyssac et al. (2002b). For very disordered graphitic carbon that is found in least metamorphosed rocks, we assign T < 200 °C.

Table 2: Zircon fission-track data from Belledonne and Grandes Rousses massifs, western Alps. All samples were counted at 1250 x dry (x 100 objective, 1.25 tube factor, 10 oculars) by J.B. Girault using a zeta (IRMM541) of 120.42 ± 3.23 (± 1SE); all ages are reported as central ages (Galbraith and Laslett, 1993). GPS coordinates in WGS84 system. Massif: NBDi = North Belledonne internal unit; NBDe = North Belledonne external unit, CBD = Central Belledonne, SBD = South Belledonne, GR =Grandes Rousses; N = number of grains counted; ρ_s = spontaneous track density; ρ_i = induced track density; N_s, N_i = number of tracks counted to determine the reported track densities; $P(\chi^2)$ = Chi-square probability that the single grain ages represent one population.

Table 3: Apatite fission-track data from Belledonne massif, western Alps. All samples were counted at 1250 x dry (x 100 objective, 1.25 tube factor, 10 oculars) by M. Balvay using a zeta (CN-5) of 273.35 ± 12.05 (± 1SE); all ages are reported as central ages (Galbraith and Laslett, 1993). Latitude and Longitude in WGS84 reference frame. Massif: NBDi = North Belledonne internal unit; NBDe = North Belledonne external unit, CBD = Central

Belledonne, SBD = South Belledonne, GR =Grandes Rousses; N = number of grains counted; ρ_s = spontaneous track density; ρ_i = induced track density; N_s, N_i = number of tracks counted to determine the reported track densities; $P(\chi^2)$ = Chi-square probability that the single grain ages represent one population.

Table 4: (U-Th-Sm/He) on zircons data (ZHe) from Belledonne and Grandes Rousses massifs, western Alps. Latitude and Longitude in WGS84 reference frame. Massif: NBDi = North Belledonne internal unit; NBDe = North Belledonne external unit, CBD = Central Belledonne, SBD = South Belledonne, GR =Grandes Rousses

Supplemental data 1: Age/elevation distribution of the thermochronological data (AFT, ZHe and ZFT) from (e) North External Belledonne (dark blue dots), (f) North Internal Belledonne (light blue dots) and (g) South Belledonne (yellow dots). One elevation range of LT thermochronological data was selected at ~1800m with, when possible, ZFT, ZHe and AFT data for thermal inversion modelling. (d) Grandes Rousses (purple dots) with full range scale. South Belledonne and Grandes Rousses: AFT data from Sabil (1995).

Supplemental data 2: Thermal histories modelled with HeFTy software for the (e) North Belledonne external unit at ~1800m, (f) North Belledonne external unit at 1800m and (g) South Belledonne massif at ~2200m. T–t paths are statistically evaluated and categorized by their value of goodness of fit (GOF). 'Acceptable' results, in green, correspond to a 0.05 GOF value and 'good' results, in purple, correspond to 0.5 GOF (Ketcham, 2005).

Supplemental data 3: Age/elevation distribution of zircon fission-track (ZFT) ages available for Aiguilles Rouges (Soom, 1990) and Mont Blanc (Glotzbach et al., 2011): gray diamond-shaped, Belledonne (this study): orange circle, Pelvoux – Meije massifs (van der Beek et al., 2010): yellow square, Grandes Rousses (this study): pink circle and Argentera (Bigot-Cormier et al., 2002): grey square.

Allen, P. A., Burgess, P. M., Galewsky, J., & Sinclair, H. D. (2001). Flexural-eustatic numerical model for drowning of the Eocene perialpine carbonate ramp and implications for Alpine geodynamics. *Geological Society of America Bulletin*, 15.

Allen, P. A., Crampton, S. L., & Sinclair, H. D. (1991). The inception and early evolution of the North Alpine Foreland Basin, Switzerland. *Basin Research*, *3*(3), 143-163. https://doi.org/10.1111/j.1365-2117.1991.tb00124.x

Allen, P. A., & Homewood, P. (Éds.). (1986). *Foreland basins*. Blackwell Scientific Publications.

Anderson, A. J., Hodges, K. V., & van Soest, M. C. (2017). Empirical constraints on the effects of radiation damage on helium diffusion in zircon. Geochimica et Cosmochimica Acta, 218(Supplement C), 308–322. https://doi.org/10.1016/j.gca.2017.09.006

Ballèvre, M., Manzotti, P., & Dal Piaz, G. V. (2018). Pre-Alpine (Variscan) Inheritance : A Key for the Location of the Future Valaisan Basin (Western Alps). *Tectonics*, *37*(3), 786-817. https://doi.org/10.1002/2017TC004633

Barféty, J.C., Bordet, P., Carme, F., Debelmas, J., Meloux, M., Moniuvent, G., Mouterde, R., Sarrot-reynauld, J., (1972). Carte géologique de la france à 1/50 000: Vizille (feuille 797) (Orléans).

Barféty, J.C., Gidon, M., Ménot, R.-P., Debon, F., (2000). Carte géologique de la france à 1/50 000: Domène (feuille 773). Second ed. (Orléans).

Bauville, A., & Schmalholz, S. M. (2015). Transition from thin- to thick-skinned tectonics and consequences for nappe formation : Numerical simulations and applications to the Helvetic nappe system, Switzerland. *Tectonophysics*, *665*, 101-117. https://doi.org/10.1016/j.tecto.2015.09.030

Beck, C., Deville, E., Blanc, E., Philippe, Y., & Tardy, M. (1998). Horizontal shortening control of Middle Miocene marine siliciclastic accumulation (Upper Marine Molasse) in the southern termination of the Savoy Molasse Basin (northwestern Alps/southern Jura). *Geological Society, London, Special Publications*, *134*(1), 263-278. https://doi.org/10.1144/GSL.SP.1998.134.01.12

Becker, A. (2000). The Jura Mountains—An active foreland fold-and-thrust belt? *Tectonophysics*, *321*(4), 381-406. https://doi.org/10.1016/S0040-1951(00)00089-5

Bellahsen, N., Jolivet, L., Lacombe, O., Bellanger, M., Boutoux, A., Garcia, S., Mouthereau, F., Le Pourhiet, L., & Gumiaux, C. (2012). Mechanisms of margin inversion in the external Western Alps : Implications for crustal rheology. *Tectonophysics*, *560-561*, 62-83. https://doi.org/10.1016/j.tecto.2012.06.022

Bellahsen, N., Mouthereau, F., Boutoux, A., Bellanger, M., Lacombe, O., Jolivet, L., & Rolland, Y. (2014). Collision kinematics in the western external Alps : Kinematics of the Alpine collision. *Tectonics*, *33*(6), 1055-1088. https://doi.org/10.1002/2013TC003453

Bellanger, M., Augier, R., Bellahsen, N., Jolivet, L., Monié, P., Baudin, T., & Beyssac, O. (2015). Shortening of the European Dauphinois margin (Oisans Massif, Western Alps) : New insights from RSCM maximum temperature estimates and 40Ar/39Ar in situ dating. *Journal of Geodynamics*, *83*, 37-64. https://doi.org/10.1016/j.jog.2014.09.004

Bellanger, M., Bellahsen, N., Jolivet, L., Baudin, T., Augier, R., & Boutoux, A. (2014). Basement shear zones development and shortening kinematics in the Ecrins Massif, Western Alps. *Tectonics*, *33*(2), 84-111. https://doi.org/10.1002/2013TC003294

Berger, A., Engi, M., Erne-Schmid, S., Glotzbach, C., Spiegel, C., de Goede, R., & Herwegh, M. (2020). The relation between peak metamorphic temperatures and subsequent cooling during continent–continent collision (western Central Alps, Switzerland). *Swiss Journal of Geosciences*, *113*(1), 4. https://doi.org/10.1186/s00015-020-00356-4

Berger, J. P. (1992). Correlative chart of the European Oligocene and Miocene : Application to the Swiss Molasse Basin. *Eclogae Geologicae Helvetiae*, *85*(3), 573-609. https://doi.org/10.5169/seals-167022

Berger, J. P. (1996). Cartes paléogéographiques-palinspastiques du bassin molassique suisse (Oligocène inférieur-Miocène moyen). *Neues Jahrbuch für Geologie und Paläontologie-Abhandlungen*, 1-44.

Berger, J. P., Reichenbacher, B., Becker, D., Grimm, M., Grimm, K., Picot, L., Storni, A., Pirkenseer, C., Derer, C., & Schaefer, A. (2005). Paleogeography of the Upper Rhine Graben (URG) and the Swiss Molasse Basin (SMB) from Eocene to Pliocene. *International Journal of Earth Sciences*, *94*(4), 697-710. https://doi.org/10.1007/s00531-005-0475-2

Bernet, M., Brandon, M., Garver, J., Balestieri, M. L., Ventura, B., & Zattin, M. (2009). Exhuming the Alps through time : Clues from detrital zircon fission-track thermochronology. *Basin Research*, *21*(6), 781-798. https://doi.org/10.1111/j.1365-2117.2009.00400.x

Bernet, M., Zattin, M., Garver, J. I., Brandon, M. T., & Vance, J. A. (2001). Steady-state exhumation of the European Alps. *Geology*, *29*(1), 35-38.

Beyssac, O., Brunet, F., Petitet, J.-P., Goffé, B., & Rouzaud, J.-N. (2004). Experimental study of the microtextural and structural transformations of carbonaceous materials under pressure and temperature. *European Journal of Mineralogy*, *15*(6), 937-951. https://doi.org/10.1127/0935-1221/2003/0015-0937

Beyssac, O., Goffé, B., Chopin, C., & Rouzaud, J. N. (2002). Raman spectra of carbonaceous material in metasediments : A new geothermometer. *Journal of Metamorphic Geology*, *20*(9), 859-871. https://doi.org/10.1046/j.1525-1314.2002.00408.x

Beyssac, O., Goffé, B., Petitet, J.-P., Froigneux, E., Moreau, M., & Rouzaud, J.-N. (2003). On the characterization of disordered and heterogeneous carbonaceous materials by Raman spectroscopy. *Spectrochimica Acta Part A. Molecular and Biomolecular Spectroscopy*, *59*(10), 2267-2276. https://doi.org/10.1016/S1386-1425(03)00070-2

Beyssac, O., Rouzaud, J. N., Goffé, B., Brunet, F., & Chopin, C. (2002). Graphitization in a high-pressure, low-temperature metamorphic gradient : A Raman microspectroscopy and HRTEM study. *Contributions to Mineralogy and Petrology*, *143*(1), 19-31. https://doi.org/10.1007/s00410-001-0324-7

Bigot-Cormier, F., Poupeau, G., & Sosson, M. (2000). Dénudations différentielles du massif cristallin externe alpin de l'Argentera (Sud-Est de la France) révélées par thermochronologie traces de fission (apatites, zircons). *Comptes Rendus de l'Académie des Sciences - Series IIA - Earth and Planetary Science*, *330*(5), 363-370. https://doi.org/10.1016/S1251-8050(00)00127-0

Billant, J., Hippolyte, J. C., & Bellier, O. (2015). Tectonic and geomorphic analysis of the Belledonne border fault and its extensions, Western Alps. Tectonophysics, 659, 31-52.

Bogdanoff, S., Michard, A., Mansour, M., & Poupeau, G. (2000). Apatite fission track analysis in the Argentera massif : Evidence of contrasting denudation rates in the External Crystalline Massifs of the Western Alps. *Terra Nova*, *12*(3), 117-125. https://doi.org/10.1046/j.1365-3121.2000.123281.x

Bodelle, J., Goguel, J., (1980). Carte géologique de la France et de la marge continentale (1/1 500 000., Orléans).

Bordet, P., & Bordet, C. (1963). Belledonne-Grandes Rousses et Aiguilles Rouges-Mont Blanc: quelques données nouvelles sur leurs rapports structuraux. Livre à la mémoire du Professeur P. Fallot».–Mém. hs Soc. géol. Fr., II, 309-320.

Bosch, G., Teixell, A., Jolivet, M., Labaume, P., Stockli,D., Domènech, M., & Monié,P. (2016). Timing of Eocene–Miocene thrustactivityin the Western Axial Zone and Chaînons Béarnais (west-Central Pyrenees) revealed by multi-method thermochronology. Comptes Rendus Geoscience, 348(3–4), 246–256. https://doi.org/10.1016/j.crte.2016.01.001

Bousquet, R., Schmid, S. M., Zeilinger, G., Oberhänsli, R., Rosenberg, C., Molli, G., Robert, C., and Rossi, P. (2012). Tectonic framework of the Alps = Carte tectonique des Alpes. University of Basel.

Boutoux, A., Bellahsen, N., Nanni, U., Pik, R., Verlaguet, A., Rolland, Y., & Lacombe, O. (2016). Thermal and structural evolution of the external Western Alps : Insights from (U–Th–Sm)/He thermochronology and RSCM thermometry in the Aiguilles Rouges/Mont Blanc massifs. *Tectonophysics*, *683*, 109-123. https://doi.org/10.1016/j.tecto.2016.06.010

Braun, J., Van Der Beek, P., Valla, P., Robert, X., Herman, F., Glotzbach, C., ... & Prigent, C. (2012). Quantifying rates of landscape evolution and tectonic processes by thermochronology and numerical modeling of crustal heat transport using PECUBE. *Tectonophysics*, *524*, 1-28.

Bucher, S., Ulardic, C., Bousquet, R., Ceriani, S., Fügenschuh, B., Gouffon, Y., & Schmid, S. M. (2004). Tectonic evolution of the Briançonnais units along a transect (ECORS-CROP) through the Italian-French Western Alps. Eclogae Geologicae Helvetiae, 97(3), 321-345. https://doi.org/10.1007/s00015-004-1139-0

Burkhard, M., & Sommaruga, A. (1998). Evolution of the western Swiss Molasse basin : Structural relations with the Alps and the Jura belt. *Geological Society, London, Special Publications*, *134*(1), 279-298. https://doi.org/10.1144/GSL.SP.1998.134.01.13

Cardello, G. L., Di Vincenzo, G., Giorgetti, G., Zwingmann, H., & Mancktelow, N. (2019). Initiation and development of the Pennine Basal Thrust (Swiss Alps): a structural and geochronological study of an exhumed megathrust. *Journal of Structural Geology*, *126*, 338-356.

Callec Y. (2001) - La déformation synsédimentaire des bassins paléogènes de l'Arc de Castellane (Annot, Barrême, Saint-Antonin). Thèse Doct. “Dynamique et Ressources des Bassins Sédimentaires”, Ecole des Mines de Paris - Mém. Sci. de la Terre, ENSMP, Paris, 43, vol. texte 347 p. + vol. figures.

Carrapa, B., Di Giulio, A., Mancin, N., Stockli, D., Fantoni, R., Hughes, A., & Gupta, S. (2016). Tectonic significance of Cenozoic exhumation and foreland basin evolution in the Western Alps. *Tectonics*, *35*(8), 1892-1912. https://doi.org/10.1002/2016TC004132

Cederbom, C. E., Sinclair, H. D., Schlunegger, F., & Rahn, M. K. (2004). Climate-induced rebound and exhumation of the European Alps. *Geology*, *32*(8), 709. https://doi.org/10.1130/G20491.1

Cederbom, C. E., van der Beek, P., Schlunegger, F., Sinclair, H. D., & Oncken, O. (2011). Rapid extensive erosion of the North Alpine foreland basin at 5-4 Ma : Rapid extensive erosion of the North Alpine foreland basin. *Basin Research*, *23*(5), 528-550. https://doi.org/10.1111/j.1365-2117.2011.00501.x

Cenki-Tok, B., Darling, J. R., Rolland, Y., Dhuime, B., & Storey, C. D. (2014). Direct dating of mid-crustal shear zones with synkinematic allanite : New *in situ* U-Th-Pb geochronological approaches applied to the Mont Blanc massif. *Terra Nova*, *26*(1), 29-37. https://doi.org/10.1111/ter.12066

Ceriani, S., & Schmid, S. M. (2004). From NS collision to WNW-directed post-collisional thrusting and folding: Structural study of the Frontal Penninic Units in Savoie (Western Alps, France). Eclogae Geologicae Helvetiae, 97(3), 347-369.

Challandes, N., Marquer, D., & Villa, I. M. (2008). P-T-t modelling, fluid circulation, and 39Ar-40Ar and Rb-Sr mica ages in the Aar Massif shear zones (Swiss Alps). *Swiss Journal of Geosciences*, *101*(2), 269-288. https://doi.org/10.1007/s00015-008-1260-6

Charollais, J., Weidmann, M., Berger, J.-P., Engesser, B., Hotellier, J.-F., Gorin, G., Reichenbacher, B., & Schäfer, P. (2007). La Molasse du bassin franco-genevois. *Archives des Sciences (Geneve)*, *60*, 59-174.

Chopin, C. (1987). Very-high-pressure metamorphism in the Western Alps: implications for subduction of continental crust [and Discussion]. Philosophical Transactions of the Royal Society of London. Series A, Mathematical and Physical Sciences, 321(1557), 183-197. doi:10.1098/rsta.1987.0010

Cordey, F., Tricart, P., Guillot, S., & Schwartz, S. (2012). Dating the Tethyan Ocean in the Western Alps with radiolarite pebbles from synorogenic Oligocene molasse basins (southeast France). *Swiss Journal of Geosciences*, *105*(1), 39-48.

Corsini, M., Ruffet, G., & Caby, R. (2004). Alpine and late-Hercynian geochronological constraints in the Argentera Massif (Western Alps). *Eclogae Geologicae Helvetiae*, *97*(1), 3-15. https://doi.org/10.1007/s00015-004-1107-8

Crampton, S.L., and Allen, P.A., 1995, Recognition of flexural forebulge unconformities associated with early stage foreland basin development: Example from the North Alpine foreland basin: American Association of Petroleum Geologists Bulletin, v. 79, p. 1495–1514.

Crouzet, C., Ménard, G., & Rochette, P. (1999). High-precision three-dimensional paleothermometry derived from paleomagnetic data in an Alpine metamorphic unit. *Geology*, *27*(6), 503-506.

Crouzet, C., Ménard, G., & Rochette, P. (2001). Cooling history of the Dauphinoise Zone (Western Alps, France) deduced from the thermopaleomagnetic record : Geodynamic implications. *Tectonophysics*, *340*(1-2), 79-93. https://doi.org/10.1016/S0040-1951(01)00142-1

Crumeyrolle P., Rubino J.L. & Clauzon G. (1991) - Miocene depositional sequences within a tectonically controlled transgressive-regressive cycle. in "Sedimentation, Tectonics and Eustasy. Sea level changes at active margins", D.I.M. Macdonald ed., Int. Ass. Sediment, Spec. Publ., 12, Oxford, p. 373-390

Debon, F., Cocherie, A., Ménot, R.-P., Vivier, G., & Barfety, J.-C. (1994). Dating of the Variscan magnesian plutonism of the external crystalline massifs of the Alps the Sept Laux granite (Belledone massif, France). *Comptes Rendus de l'Académie des Sciences - Series IIA - Earth and Planetary Science*, *318*(11), 10.

Debon, F., Guerrot, C., Ménot, R.-P., Vivier, G., & Cocherie, A. (1998). Late Variscan granites in the Belledonne massif (French Western Alps): An Early Visean magnesian plutonism. Schweizerische Mineralogische und Petrographische Mitteilungen, 78, 67–85.

Debon, F. & Lemmet, M. (1999). Evolution of Mg/Fe ratios in late Variscan plutonic rocks from the external crystalline massifs of the Alps (France, Italy, Switzerland). Journal of Petrology, 40(7), 1151-1185.

DeCelles, P. G., & Giles, K. A. (1996). Foreland basin systems. Basin research, 8(2), 105-123.

Demarcq, G., Perriaux, J. et al. (1984). Néogène. *In:* Debrand-Passard, S., Courbouleix, S. & Lienhardt, M. J. (eds) *Synthèse géologique du Sud-Est de la France*. Mémoires du Bureau de Recherches Géologiques et Minières, 125, 469-519.

Demarcq, G. (1970). Etude stratigraphique du Miocène rhodanien (*Doctoral dissertation*, BRGM).

Demeulemeester, P. (1986). Demeulemeester et al. - 1986—Influence du métamorphisme alpin sur les âges isotopiques RbSr et KAr des biotites des massifs cristallins externes (Alpes françaises).pdf. *Géologie Alpine*, *62*, 31-44.

Deville, E., Blanc, E., Tardy, M., Beck, C., Cousin, M., & Ménard, G. (1994). Thrust Propagation and Syntectonic Sedimentation in the Savoy Tertiary Molasse Basin (Alpine Foreland). In A. Mascle (Éd.), *Hydrocarbon and Petroleum Geology of France* (p. 269-280). Springer Berlin Heidelberg. https://doi.org/10.1007/978-3-642-78849-9_19

Deville, É., & Chauvière, A. (2000). Thrust tectonics at the front of the western Alps : Constraints provided by the processing of seismic reflection data along the Chambéry transect. *Comptes Rendus de l'Académie des Sciences - Series IIA - Earth and Planetary Science*, *331*(11), 725-732. https://doi.org/10.1016/S1251-8050(00)01463-4

Deville, E., & Sassi, W. (2006). Contrasting thermal evolution of thrust systems : An analytical and modeling approach in the front of the western Alps. *AAPG Bulletin*, *90*(6), 887-907. https://doi.org/10.1306/01090605046

Dumitru, T.A., (1993). A new computer-automated microscope stage system for fission-track analysis. Nuclear Tracks and Radiation Measurements 21, 575–580. https://doi.org/10.1016/1359-0189(93)90198-I

Dumont, T., Schwartz, S., Guillot, S., Simon-Labric, T., Tricart, P., & Jourdan, S. (2012). Structural and sedimentary records of the Oligocene revolution in the Western Alpine arc. Journal of Geodynamics, 56, 18-38. https://doi.org/10.1016/j.jog.2011.11.006

Dumont, T., Champagnac, J.-D., Crouzet, C., & Rochat, P. (2008). Multistage shortening in the Dauphiné zone (French Alps) : The record of Alpine collision and implications for pre-Alpine restoration. *Swiss Journal of Geosciences*, *101*(S1), 89-110. https://doi.org/10.1007/s00015-008-1280-2

Egli, D., Mancktelow, N., & Spikings, R. (2017). Constraints from 40Ar/39Ar geochronology on the timing of Alpine shear zones in the Mont Blanc-Aiguilles Rouges region of the European Alps. *Tectonics*, *36*(4), 730-748.

Egli, D., Müller, W., & Mancktelow, N. (2016). Laser-cut Rb-Sr microsampling dating of deformational events in the Mont Blanc-Aiguilles Rouges region (European Alps). *Terra Nova*, *28*(1), 35-42. https://doi.org/10.1111/ter.12184

Erdös, Z., Huismans, R. S., & Van der Beek, P. (2019). Control of increased sedimentation on orogenic fold-and-thrust belt structure–insights into the evolution of the Western Alps. *Solid Earth*, *10*(2), 391-404. https://doi.org/10.5194/se-10-391-2019

Fauquette, S., Bernet, M., Suc, J.-P., Grosjean, A.-S., Guillot, S., van der Beek, P., Jourdan, S., Popescu, S.-M., Jiménez-Moreno, G., Bertini, A., Pittet, B., Tricart, P., Dumont, T., Schwartz, S., Zheng, Z., Roche, E., Pavia, G., & Gardien, V. (2015). Quantifying the Eocene to Pleistocene topographic evolution of the southwestern Alps, France and Italy. *Earth and Planetary Science Letters*, *412*, 220-234. https://doi.org/10.1016/j.epsl.2014.12.036

Fernandez, A., Guillot, S., Ménot, R.-P., & Ledru, P. (2002). Late Paleozoic polyphased tectonics in the SW Belledonne massif (external crystalline massifs, French Alps). *Geodinamica Acta*, *15*(2), 127-139. https://doi.org/10.1080/09853111.2002.10510746

Flowers, R. M., Ketcham, R. A., Shuster, D. L., & Farley, K. A. (2009). Apatite (U–Th)/He thermochronometry using a radiation damage accumulation and annealing model. Geochimica et Cosmochimica Acta, 73(8), 2347–2365. https://doi.org/10.1016/j.gca.2009.01.015

Ford, M., & Lickorish, W. H. (2004). Foreland basin evolution around the western Alpine Arc. *Geological Society, London, Special Publications*, *221*(1), 39-63.

Ford, M., Duchêne, S., Gasquet, D., & Vanderhaeghe, O. (2006). Two-phase orogenic convergence in the external and internal SW Alps. *Journal of the Geological Society*, *163*(5), 815-826. https://doi.org/10.1144/0016-76492005-034

Fréville, K., Trap, P., Faure, M., Melleton, J., Li, X.-H., Lin, W., Blein, O., Faure, O., & Poujol, M. (2018). Structural, metamorphic and geochronological insights on the Variscan evolution of the Alpine basement in the Belledonne Massif (France). *Tectonophysics*, *726*, 14-42. https://doi.org/10.1016/j.tecto.2018.01.017

Fügenschuh, B., & Schmid, S. M. (2003). Late stages of deformation and exhumation of an orogen constrained by fission-track data : A case study in the Western Alps. *Geological Society of America Bulletin*, *115*(11), 1425. https://doi.org/10.1130/B25092.1

Gabalda, S., Beyssac, O., Jolivet, L., Agard, P., & Chopin, C. (2009). Thermal structure of a fossil subduction wedge in the Western Alps. Terra Nova, 21(1), 23-34.

Gallagher, K., Brown, R., & Johnson, C. (1998). Fission track analysis and its applications to geological problems. Annual Review of Earth and Planetary Sciences, 26(1), 519–572. https://doi.org/10.1146/annurev.earth.26.1.519

Galbraith, R. F., & Laslett, G. M. (1993). Statistical models for mixed fission track ages. Nuclear tracks and radiation measurements, 21(4), 459-470.

Garefalakis, P., & Schlunegger, F. (2019). Tectonic processes, variations in sediment flux, and eustatic sea level recorded by the 20Myr old Burdigalian transgression in the Swiss Molasse basin. *Solid Earth*, *10*(6), 2045-2072. https://doi.org/10.5194/se-10-2045-2019

Garver, A.J.I., Reiners, P.W., Walker, L.J., Ramage, J.M., Perry, S.E., 2005. Implications for timing of Andean uplift from thermal resetting of radiation-damaged zircon in the Cordillera Huayhuash, Northern Peru. J. Geol. 113, 117–138. http://dx.doi.org/10.1086/427664.

Gautheron, C., Djimbi, D. M., Roques, J., Balout, H., Ketcham, R. A., Simoni, E., Pik R., Seydoux-Guillaume A. M. & Tassan-Got, L. (2020). A multi-method, multi-scale theoretical study of He and Ne diffusion in zircon. *Geochimica et Cosmochimica Acta*, *268*, 348-367.

Girault, J. B., Bellahsen, N., Boutoux, A., Rosenberg, C. L., Nanni, U., Verlaguet, A., & Beyssac, O. (2020). The 3-D Thermal Structure of the Helvetic Nappes of the European Alps : Implications for Collisional Processes. *Tectonics*, *39*(3). https://doi.org/10.1029/2018TC005334

Gleadow, A. J. W., Hurford, A. J., & Quaife, R. D. (1976). Fission track dating of zircon : Improved etching techniques. *Earth and Planetary Science Letters*, *33*(2), 273-276. https://doi.org/10.1016/0012-821X(76)90235-1

Glotzbach, C., Reinecker, J., Danišík, M., Rahn, M., Frisch, W., Spiegel, C., 2008. Neogene exhumation history of the Mont Blanc massif, western Alps. Tectonics 27, TC4011. http://dx.doi.org/10.1029/2008TC002257.

Glotzbach, C., van der Beek, P.A., Spiegel, C., 2011. Episodic exhumation and relief growth in the Mont Blanc massif, Western Alps from numerical modelling of thermochronology data. Earth Planet. Sci. Lett. 304, 417–430. http://dx.doi.org/10.1016/j.epsl.2011.02.020.

Gorin, G., Signer, C., & Ameerger, G. (1993). Structural configuration of the western Swiss Molasse Basin as defined by reflection seismic data. *Eclogae Geologicae Helvetiae*, *86*(3), 693-716. https://doi.org/10.5169/seals-167259

Gratier, J.-P., Lejeune, B., & Vergne, J. L. (1973). *Etude des déformations de la couverture et des bordures sédimentaires des massifs cristallins externes de Belledonne,des Grandes Rousses et du Pelvoux (depuis Les Aravis jusqu'à La région de Remollon). Alpes françaises* [Université Joseph Fourier de Grenoble]. https://tel.archives-ouvertes.fr/tel-00460985

Grosjean, A. S., Pittet, B., Gardien, V., Leloup, P. H., Mahéo, G., & Bailleza Garcia, J. (2017). Tectonic heritage in drainage pattern and dynamics: the case of the French South Alpine Foreland Basin (ca. 45–20 Ma). *Basin Research*, *29*, 26-50.

Guillot, S., Ménot, R.-P., (2009). Paleozoic evolution of the External Crystalline Massifs of the Western Alps. Compt. Rendus Geosci. 341, 253–265. http://dx.doi.org/10.1016/j.crte.2008.11.010.

Guenthner, W. R., Reiners, P. W., Ketcham, R. A., Nasdala, L., & Giester, G. (2013). Helium diffusion in natural zircon : Radiation damage, anisotropy, and the interpretation of zircon (U-Th)/He thermochronology. *American Journal of Science*, *313*(3), 145-198. https://doi.org/10.2475/03.2013.01

Guenthner, W. R., Reiners, P. W., & Tian, Y. (2014). Interpreting date–eU correlations in zircon (U-Th)/He datasets: A case study from the Longmen Shan, China. Earth and Planetary Science Letters, 403, 328–339. https://doi.org/10.1016/j.epsl.2014.06.050

Guenthner, W. R., Reiners, P. W., DeCelles, P. G., & Kendall, J. (2015). Sevier belt exhumation in central Utah constrained from complex zircon (U-Th)/He data sets: Radiation damage and He inheritance effects on partially reset detrital zircons. Geological Society of America Bulletin, 127(3–4), 323–348. https://doi.org/10.1130/B31032.1

Guenthner, W. R., Reiners, P. W., Drake, H., & Tillberg, M. (2017). Zircon, titanite, and apatite (U-Th)/He ages and age-eU correlations from the Fennoscandian Shield, southern Sweden: Fennoscandian Zirc He age-eU correlation. Tectonics, 36, 1254–1274. https://doi.org/ 10.1002/2017TC004525

Herwegh, M., Berger, A., Glotzbach, C., Wangenheim, C., Mock, S., Wehrens, P., Baumberger, R., Egli, D., & Kissling, E. (2020). Late Stages of Continent-Continent Collision : Timing, Kinematic Evolution, and Exhumation of the Northern Rim (Aar Massif) of the Alps. *Earth-Science Reviews*, *200*, 102959. https://doi.org/10.1016/j.earscirev.2019.102959

Hurford, A.J., Green, P.F., (1983). The zeta age calibration of fission-track dating. Chemical Geology 41, 285–317. https://doi.org/10.1016/S0009-2541(83)80026-6

Johnson, J. E., Flowers, R. M., Baird, G. B., & Mahan, K. H. (2017). "Inverted" zircon and apatite (U–Th)/He dates from the Front Range, Colorado: High-damage zircon as a low-temperature (<50 °C) thermochronometer. Earth and Planetary Science Letters, 466 (supplement C), 80–90. https://doi.org/10.1016/j.epsl.2017.03.002

Jourdan, S., Bernet, M., Schwartz, S., Guillot, S., Tricart, P., Chauvel, C., Dumont, T., Montagnac, G., & Bureau, S. (2012). Tracing the Oligocene-Miocene Evolution of the Western Alps Drainage Divide with Pebble Petrology, Geochemistry, and Raman Spectroscopy of Foreland Basin Deposits. *The Journal of Geology*, *120*(6), 603-624. https://doi.org/10.1086/667813

Kalifi, A., Philippe, S., Philippe-Hervé, L., Vincenzo, S., Bastien, H., Albert, G., ... & Bernard, P. (2020). Changes in hydrodynamic process dominance (wave, tide or river) in foreland sequences: The subalpine Miocene Molasse revisited (France). *Sedimentology*.

Kempf, O., Matter, A., Burbank, D. W., & Mange, M. (1999). Depositional and structural evolution of a foreland basin margin in a magnetostratigraphic framework : The eastern Swiss Molasse Basin. *International Journal of Earth Sciences*, *88*(2), 253-275. https://doi.org/10.1007/s005310050263

Kempf, Schlunegger, Strunck, & Matter. (1998). Palaeomagnetic evidence for late Miocene rotation of the Swiss Alps : Results from the north Alpine foreland basin. *Terra Nova*, *10*(1), 6-10. https://doi.org/10.1046/j.1365-3121.1998.00164.x

Ketcham, R.A., Gautheron, C., Tassan-Got, L., 2011. Accounting for long alpha-particle stopping distances in (U–Th–Sm)/He geochronology: refinement of the baseline case. Geochim. Cosmochim. Acta 75, 7779–7791. http://dx.doi.org/10.1016/j.gca.2011.10.011.

Ketcham, R. A. (2005). Forward and Inverse Modeling of Low-Temperature Thermochronometry Data. *Reviews in Mineralogy and Geochemistry*, *58*(1), 275-314. https://doi.org/10.2138/rmg.2005.58.11

Kiss, D., Duretz, T., & Schmalholz, S. M. (2019). *Towards a nappe theory : Thermo-mechanical simulations of nappe detachment, transport and stacking in the Helvetic Nappe System, Switzerland* [Preprint]. Tectonic plate interactions, magma genesis, and lithosphere deformation at all scales/Structural geology and tectonics, rock physics, experimental deformation/Tectonics. https://doi.org/10.5194/se-2019-130

Kuhlemann, J., Frisch, W., Székely, B., Dunkl, I., & Kazmer, M. (2002). Post-collisional sediment budget history of the Alps : Tectonic versus climatic control. *International Journal of Earth Sciences*, *91*(5), 818-837. https://doi.org/10.1007/s00531-002-0266-y

Kuhlemann, J., & Kempf, O. (2002). Post-Eocene evolution of the North Alpine Foreland Basin and its response to Alpine tectonics. *Sedimentary Geology*, *152*(1-2), 45-78. https://doi.org/10.1016/S0037-0738(01)00285-8

Lafosse, M., Boutoux, A., Bellahsen, N., & Le Pourhiet, L. (2016). Role of tectonic burial and temperature on the inversion of inherited extensional basins during collision. *Geological Magazine*, *153*(5-6), 811-826. https://doi.org/10.1017/S0016756816000510

Lahfid, A., Beyssac, O., Deville, E., Negro, F., Chopin, C., & Goffé, B. (2010). Evolution of the Raman spectrum of carbonaceous material in low-grade metasediments of the Glarus Alps (Switzerland) : RSCM in low-grade metasediments. *Terra Nova*, *22*(5), 354-360. https://doi.org/10.1111/j.1365-3121.2010.00956.x

Laubscher, H. P. (1981). The 3D propagation of decollement in the Jura. *Geological Society, London, Special Publications*, *9*(1), 311-318.

Lelarge, M. L. (1993). *Thermochronologie par la méthode des traces de fission d'une marge passive (dôme de Ponta Grossa, SE Brésil) et au sein d'une chaîne de collision (zone externe de l'arc alpin, France)* [Université Joseph Fourier de Grenoble]. https://tel.archives-ouvertes.fr/tel-00603209

Leloup, P. H., Arnaud, N., Sobel, E. R., & Lacassin, R. (2005). Alpine thermal and structural evolution of the highest external crystalline massif : The Mont Blanc. *Tectonics*, *24*(4). https://doi.org/10.1029/2004TC001676

Lemoine, M., Bas, T., Arnaud-Vanneau, A., Arnaud, H., Dumont, T., Gidon, M., Bourbon, M., de Graciansky, P.-C., Rudkiewicz, J.-L., Megard-Galli, J., & Tricart, P. (1986). The continental margin of the Mesozoic Tethys in the Western Alps. *Marine and Petroleum Geology*, *3*(3), 179-199. https://doi.org/10.1016/0264-8172(86)90044-9

Looser, N., Madritsch, H., Guillong, M., Laurent, O., Wohlwend, S., & Bernasconi, S. M. (2021). Absolute Age and Temperature Constraints on Deformation Along the Basal Décollement of the Jura Fold-and-Thrust Belt From Carbonate U-Pb Dating and Clumped Isotopes. *Tectonics*, *40*(3), e2020TC006439.

Malusà, M. G., Polino, R., Zattin, M., Bigazzi, G., Martin, S., & Piana, F. (2005). Miocene to Present differential exhumation in the Western Alps : Insights from fission track thermochronology: EXHUMATION IN THE WESTERN ALPS. *Tectonics*, *24*(3). https://doi.org/10.1029/2004TC001782

Mangenot, X., Deçoninck, J.-F., Bonifacie, M., Rouchon, V., Collin, P.-Y., Quesne, D., Gasparrini, M., & Sizun, J.-P. (2019). Thermal and exhumation histories of the northern subalpine chains (Bauges and Bornes-France) : Evidence from forward thermal modeling coupling clay mineral diagenesis, organic maturity and carbonate clumped isotope (Δ_{47}) data: XXXX. *Basin Research*, *31*(2), 361-379. https://doi.org/10.1111/bre.12324

Mark, C., Cogné, N., & Chew, D. (2016). Tracking exhumation and drainage divide migration of the Western Alps : A test of the apatite U-Pb thermochronometer as a detrital provenance tool. *Geological Society of America Bulletin*, *1*, 23. https://doi.org/10.1130/B31351.

Marquer, D., Calcagno, P., Barfety, J.-C., & Baudin, T. (2006). 3D Modeling and Kinematics of the External Zone of the French Western Alps (Belledonne and Grand Châtelard Massifs, Maurienne Valley, Savoie). *Eclogae Geologicae Helvetiae*, *99*(2), 211-222. https://doi.org/10.1007/s00015-006-1183-z

Mastrangelo, B., Charollais, J., Wernli, R., & Metzger, J. (2013). Accidents longitudinaux dans la Molasse rouge auct. Et dans son substratum sur le versant oriental du Salève (Haute-Savoie, France). *Swiss Journal of Geosciences*, *106*(2), 253-263. https://doi.org/10.1007/s00015-013-0136-6

Matter, A., Homewood, P. W., Caron, C., Van Stuijvenberg, J., Weidmann, M., & Winkler, W. (1980). Flysch and molasse of central and western Switzerland. Geology of Switzerland, a guide book: Schweiz Geologica Kommission, 261-293.

Meckel, L. D., Ford, M., & Bernoulli, D. (1996). Tectonic and sedimentary evolution of the Dévoluy Basin, a remnant of the Tertiary western Alpine foreland basin, SE France. *Géol. de la France*, *2*, 3-26.

Ménot, R.-P., (1988). An overview of the geology of the Belledonne Massif (external crystalline massifs of Western Alps). Schweiz. Mineral. Petrogr. Mitt. 70, 33–53

Morend D. (2000). High-resolution seismic facies of alluvial depositional systems in the Lower Freshwater Molasse (Oligocene-early Miocene, western Swiss Molasse Basin). Terre et Environnement, Genève, 23:1-97

Mosar, J. (1999). Present-day and future tectonic underplating in the western Swiss Alps : Reconciliation of basement/wrench-faulting and décollement folding of the Jura and Molasse basin in the Alpine foreland. *Earth and Planetary Science Letters*, *173*(3), 143-155. https://doi.org/10.1016/S0012-821X(99)00238-1

Moscariello, A., Gorini, G., Charollais, J., & Russillon, E. (2014). *Geology of Western Switzerland and nearby France in a Geo-Energy perspective* (p. 26).

Nibourel, L., Berger, A., Egli, D., Luensdorf, N. K., & Herwegh, M. (2018). Large vertical displacements of a crystalline massif recorded by Raman thermometry. *Geology*, *46*(10), 879-882. https://doi.org/10.1130/G45121.1

Nziengui, J. J. (1993). *Excès d'argon radiogénique dans les quartz des fissures tectoniques : Implications pour la datation des séries métamorphiques. L'exemple de la coupe de la Romanche, Alpes Occidentales françaises* [Université Joseph Fourier de Grenoble]. https://tel.archives-ouvertes.fr/tel-00452118

Paquette, J.-L., Ménot, R.-P., Peucat, J.-J., (1989). REE, Sm-Nd and U-Pb zircon study of eclogites from the Alpine External Massifs (Western Alps): evidence for crustal contamination. Earth Planet. Sci. Lett. 96, 181–198

Philippe, Y. (1995). *Rampes latérales et zones de transfert dans les chaînes plissées : Géométrie, condition de formation et pièges structuraux associés* [Université de Savoie]. https://tel.archives-ouvertes.fr/tel-00755680

Philippe, Y., Deville, E., & Mascle, A. (1998). Thin-skinned inversion tectonics at oblique basin margins : Example of the western Vercors and Chartreuse Subalpine massifs (SE France). *Geological Society, London, Special Publications*, *134*(1), 239-262. https://doi.org/10.1144/GSL.SP.1998.134.01.11

Powell, J., Schneider, D.,Stockli,D., & Fallas, K. (2016). Zircon (U-Th)/Hethermochronology of Neoproterozoic strata from the Mackenzie Mountains, Canada: Implications for the Phanerozoic exhumation and deformation history of the northern Canadian Cordillera. Tectonics, 35, 663–689. https://doi.org/10.1002/2015TC003989

Rahn, M.K., 1994. Incipient Metamorphism of the Glarus Alps: Petrology of the Taveyanne Greywacke and Fission Track Dating (Ph-D Thesis) Univ of Basel, Basel, Switzerland.

Rahn, M.K., Brandon, M.T., Batt, G.E., Garver, J.I., 2004. A zero-damage model for fission-track annealing in zircon. Am. Mineralineralogyst 89, 473–484.

Rigassi, D. (1996). Regional geological framework of the Pays de Gex (Jura foldbelt, Molasse basin, Bresse). Rapport inédit, 1-50, Soc. Gén.Industrie, Genève.

Rigassi, D. (1980). Couches détritiques de La London (Pays de Gex, Ain). Chez l'auteur, Genève, 11 p.

Rigassi, D. (1957). Le Tertiaire de la région genevoise et savoisienne. Bull. Ver. Schweizer. Petrol.-Geol. U. Ing. Basel, 24/66:19-34.

Rolland, Y., Cox, S., Boullier, A.-M., Pennacchioni, G., & Mancktelow, N. (2003). Rare earth and trace element mobility in mid-crustal shear zones : Insights from the Mont Blanc Massif (Western Alps). *Earth and Planetary Science Letters*, *214*(1-2), 203-219. https://doi.org/10.1016/S0012-821X(03)00372-8

Rolland, Y., Rossi, M., Cox, S. F., Corsini, M., Mancktelow, N., Pennacchioni, G., Fornari, M., & Boullier, A. M. (2008). 40Ar/39Ar dating of synkinematic white mica : Insights from fluid-rock reaction in low-grade shear zones (Mont Blanc Massif) and constraints on timing of deformation in the NW external Alps. *Geological Society, London, Special Publications*, *299*(1), 293-315. https://doi.org/10.1144/SP299.18

Rolland, Y., Cox, S. F., & Corsini, M. (2009). Constraining deformation stages in brittle–ductile shear zones from combined field mapping and 40Ar/39Ar dating : The structural evolution of the Grimsel Pass area

(Aar Massif, Swiss Alps). *Journal of Structural Geology*, *31*(11), 1377-1394. https://doi.org/10.1016/j.jsg.2009.08.003

Rossi, M., & Rolland, Y. (2014). Stable isotope and Ar/Ar evidence of prolonged multiscale fluid flow during exhumation of orogenic crust: Example from the Mont Blanc and Aar Massifs (NW Alps). Tectonics, 33(9), 1681-1709.

Rubino, J. L., Lesueur, J. L., & Clauzon, G. (1990). Le Miocène inférieur et moyen du bassin rhodanien. Stratigraphie séquentielle et sédimentologie. Field Trip Guidebook: Special Publication of the Association des Sédimentologistes Français.

Sabil, N. (1995). *La datation par traces de fission : Aspects méthodologiques et applications thermochronologiques en contexte alpin et de marge continentale.* [Université Joseph Fourier de Grenoble]. https://tel.archives-ouvertes.fr/tel-00534619

Sanchez, G., Rolland, Y., Jolivet, M., Brichau, S., Corsini, M., & Carter, A. (2011). Exhumation controlled by transcurrent tectonics : The Argentera-Mercantour massif (SW Alps): Exhumation controlled by transcurrent tectonics in SW Alps. *Terra Nova*, [illegible]. https://doi.org/10.1111/j.1365-3121.2011.00991.x

Sanchez, G., Rolland, Y., Schneider, J., Corsini, M., Oliot, E., Goncalves, P., Verati, C., Lardeaux, J.-M., & Marquer, D. (2011). Dating low-temperature deformation by 40Ar/39Ar on white mica, insights from the Argentera-Mercantour Massif (SW Alps). *Lithos*, *125*(1-2), 521-536. https://doi.org/10.1016/j.lithos.2011.03.009

Schlunegger, F., Matter, A., Burbank, D. W., Leu, W., Matter, M., & Màtyàs, J. (1997). Sedimentary sequences, seismofacies and evolution of depositional systems of the Oligo/Miocene Lower Freshwater Molasse Group, Switzerland. *Basin Research*, *9*(1), 1-26. https://doi.org/10.1046/j.1365-2117.1997.00029.x

Schlunegger, F., Slingerl, R., & Matter, A. (1998). Crustal thickening and crustal extension as controls on the evolution of the drainage network of the central Swiss Alps between 30 Ma and the present: constraints from the stratigraphy of the North Alpine Foreland Basin and the structural evolution of the Alps. *Basin Research*, *10*(2), 197-212.

Schlunegger, F., Rieke-Zapp, D., & Ramseyer, K. (2007). Possible environmental effects on the evolution of the Alps-Molasse Basin system. *Swiss Journal of Geosciences*, *100*(3), 383-405. https://doi.org/10.1007/s00015-007-1238-9

Schlunegger, F., & Kissling, E. (2015). Slab rollback orogeny in the Alps and evolution of the Swiss Molasse basin. *Nature Communications*, *6*(1), 8605. https://doi.org/10.1038/ncomms9605

Schmid, S. M., Pfiffner, O. A., Froitzheim, N., Schönborn, G., & Kissling, E. (1996). Geophysical-geological transect and tectonic evolution of the Swiss-Italian Alps. *Tectonics*, *15*(5), 1036-1064. https://doi.org/96TC00433

Seward, D., & Mancktelow, N. S. (1994). Neogene kinematics of the central and western Alps : Evidence from fission-track dating. *Geology*, *22*, 803-806.

Simeon, Y. (1979). Etude pétrologique, géochimique et structurale des terrains cristallins de Belledonne entre l'Arc et l'Isère (Alpes françaises) (Doctoral dissertation).

Simon-Labric, T. (2009). Simon-Labric et al. - 2009—40 Ar⁄ 39 Ar dating of Penninic Front tectonic displacement (W Alps) during the Lower Oligocene (31–34 Ma).pdf. *Terra Nova*, *21*(2), 127-136. https://doi.org/10.1111/j.1365-3121.2009.00865.x

Sinclair, H. D. (1996). Plan-view curvature of foreland basins and its implications for the palaeostrength of the lithosphere underlying the western Alps. *Basin Research*, *8*(2), 173-182. https://doi.org/10.1046/j.1365-2117.1996.01525.x

Sinclair, H. D. (1997). Flysch to molasse transition in peripheral foreland basins : The role of the passive margin versus slab breakoff. *Geology*, *25*(12), 123-1126.

Sinclair, H. D., & Allen, P. A. (1992). Vertical versus horizontal motions in the Alpine orogenic wedge : Stratigraphic response in the foreland basin. *Basin Research*, *4*(3-4), 215-232. https://doi.org/10.1111/j.1365-2117.1992.tb00046.x

Sissingh, W. (2001). Tectonostratigraphy of the West Alpine Foreland : Correlation of Tertiary sedimentary sequences, changes in eustatic sea-level and stress regimes. *Tectonophysics*, *333*(3-4), 361-400. https://doi.org/10.1016/S0040-1951(01)00020-8

Sissingh, W. (2006). Syn-kinematic palaeogeographic evolution of the West European Platform: correlation with Alpine plate collision and foreland deformation. Netherlands Journal of Geosciences/Geologie en Mijnbouw, 85(2), 131-180.

Spiegel, C., Kuhlemann, J., Dunkl, I., Frisch, W., Von Eynatten, H., & Balogh, K. (2000). The erosion history of the Central Alps: evidence from zircon fission track data of the foreland basin sediments. *Terra Nova*, *12*(4), 163-170.

Ternois, S., Odlum, M., Ford, M., Pik, R., Stockli, D., Tibari, B., Vacherat, A., & Bernard, V. (2019). Thermochronological Evidence of Early Orogenesis, Eastern Pyrenees, France. *Tectonics*, *38*(4), 1308-1336. https://doi.org/10.1029/2018TC005254

Tibari, B., Vacherat, A., Stab, M., Pik, R., Yeghicheyan, D., & Hild, P. (2016). An Alternative Protocol for Single Zircon Dissolution with Application to (U-Th-Sm)/He Thermochronometry. *Geostandards and Geoanalytical Research*, *40*(3), 365-375. https://doi.org/10.1111/j.1751-908X.2016.00375.x

Vacherat, A., Mouthereau, F., Pik, R., Bellahsen, N., Gautheron, C., Bernet, M., et al. (2016). Rift-to-collision transition recorded by tectonothermal evolution of the northern Pyrenees: Cooling history of the northern Pyrenees. Tectonics, 35, 907–933. https://doi.org/10.1002/2015TC004016

Vacherat, A., Mouthereau, F., Pik, R., Bernet, M., Gautheron, C., Masini, E., et al. (2014). Thermal imprint of rift-related processes in orogens as recorded in the Pyrenees. Earth and Planetary Science Letters, 408, 296–306. https://doi.org/10.1016/j.epsl.2014.10.014

van der Beek, P. A., Valla, P. G., Herman, F., Braun, J., Persano, C., Dobson, K. J., & Labrin, E. (2010). Inversion of thermochronological age–elevation profiles to extract independent estimates of denudation and relief history — II : Application to the French Western Alps. *Earth and Planetary Science Letters*, *296*(1-2), 9-22. https://doi.org/10.1016/j.epsl.2010.04.032

Vermeesch P (2009) RadialPlotter: a Java application for fission track, luminescence and other radial plots. Rad Meas 44:409–410. doi.org/10.1016/j.earscirev.2017.07.004

von Eynatten, H., & Gaupp, R. (1999). Provenance of Cretaceous synorogenic sandstones in the Eastern Alps: constraints from framework petrography, heavy mineral analysis and mineral chemistry. Sedimentary Geology, 124(1-4), 81-111.

von Raumer, J. F. (1998). The Palaeozoic evolution in the Alps: from Gondwana to Pangea. Geologische Rundschau, 87(3), 407-435.

von Raumer, J. F., & Bussy, F. (2004). Mont Blanc and Aiguilles Rouges; geology of their polymetamorphic basement (External massifs, Western Alps, France-Switzerland).

Weisenberger, T. B., Rahn, M., van der Lelij, R., Spikings, R. A., & Bucher, K. (2012). Timing of low-temperature mineral formation during exhumation and cooling in the Central Alps, Switzerland. *Earth and Planetary Science Letters*, *327-328*, 1-8. https://doi.org/10.1016/j.epsl.2012.01.007

Willett, S. D., & Schlunegger, F. (2010). The last phase of deposition in the Swiss Molasse Basin : From foredeep to negative-alpha basin: The last phase of deposition in the Swiss Molasse Basin. *Basin Research*, *22*(5), 623-639. https://doi.org/10.1111/j.1365-2117.2009.00435.x

Jean-Baptiste Girault Writing – original draft, writing review, editing, data curation and acquisition
Nicolas Bellahsen Supervision, writing - review & editing
Matthias Bernet Fission Tracks methodology, writing - review & editing
Raphael Pik (U-Th-Sm) / He methodology, writing - review & editing
Nicolas Loget Writing - review & editing
Eric Lasseur Seismic and sedimentory acquisition and discussion, writing - review & editing
Claudio Rosenberg Writing - review & editing
Mélanie Balvay Apatite fission track acquisition
Manon Sonnet Cross section discussion

Declaration of interests

☒ The authors declare that they have no known competing financial interests or personal relationships that could have appeared to influence the work reported in this paper.

☐The authors declare the following financial interests/personal relationships which may be considered as potential competing interests:

Insight into External Crystalline Massifs cooling / exhumation during the Oligo-Miocene period.
ZFT ages range between 15-20 Ma, ZHe ages between 5-12 Ma, AFT ages between 2-10 Ma.
South ECMs record an early and slow exhumation at ca. 27 whereas North ECMs record a rapid exhumation at ca. 18 Ma
18 Ma correspond to the end of the transition period between distributed and localised shortening